A study of the behavior of the diameter of the ascending aorta when hemorrhage is induced in mongrel dogs

by

Jorge Alberto García-Zuazaga

A Thesis Submitted to the
Graduate Faculty in Partial Fulfillment of the
Requirements for the Degree of
MASTER OF SCIENCE

Interdepartmental Program: Biomedical Engineering
Major: Biomedical Engineering

Iowa State University
Ames, Iowa

1995

To Mami, Papi, and Jorge Carlos

TABLE OF CONTENTS

LIST OF FIGURES

LIST OF TABLES

LIST OF EQUATIONS

CHAPTER 1: INTRODUCTION

Aortic compliance, or aortic extendibility, according to the Food and Drug Administration (FDA) definition used by medical companies, refers to the change in aortic blood volume divided by the corresponding change in aortic blood pressure.

The measurement of the compliance value can be critical in the diagnosis of the need for heart valve replacement. Aortic diameter and, ultimately, aortic compliance information is important to medical professionals for determining the feasibility of implanting a porcine heart valve instead of a mechanical artificial heart valve in the case of aortic stenosis. Some of the advantages of the porcine tissue valve over an artificial valve include a lower cost and no need for anticoagulant drugs.

Several invasive and non-invasive techniques have been used experimentally to determine aortic compliance values. Invasive examples include the use of catheters and transducers, while non-invasive examples include the use of magnetic resonance imaging (MRI), computer tomography (CT scans), or ultrasound imaging. However, there have been limited studies where a non-invasive measurement technique has been validated by correlation to measurements obtained by invasive techniques when hemorrhage is induced. Thus, this research project focused on measuring aortic diameter non-invasively (over a range of different pressures) as a first step towards the non-invasive measurement of aortic compliance.

Before attempting to determine the diameter of the aorta non-invasively, several methods of measurement were considered. Many types of medical imaging techniques

are currently available, each with its own advantages and disadvantages. One important aspect of the imaging process is real time imaging (images recorded as they occur). Since the cardiovascular system is dynamic, the equipment used must be able to record the ascending aorta as it changes its diameter during the systolic and diastolic phases of the cardiac cycle.

Magnetic resonance imaging (MRI) is a non-invasive procedure that is effective in measuring blood flow and diameter changes. Some limitations that may be expected with the MRI are that the images are not taken in real time. On the other hand, the images are in the form of a still frame (Webster, 1978).

Computerized tomography (CT) scans are another alternative for a non-invasive measuring system. The CT scan uses x-rays to obtain the images. This has a potential to be hazardous when used repeatedly, or for prolonged periods of time (Webster, 1978).

Ultrasound imaging was selected for this research since in this method the images are produced in real time. The pictures are dynamic instead of delayed and static. Cost was also a factor in the decision to use ultrasound; it is inexpensive compared to MRI and CT imaging processes.

After selecting the method for determining the aortic diameter, the next step was to understand the physiological significance of both the aortic diameter and the aortic compliance values in the cardiovascular system. For this task, the behavior of the cardiac cycle and its different mechanical events were reviewed (see Figure 1.1). The cardiac cycle was segmented into five major chronological events. These events are: late diastole, atrial systole, ventricular systole, ventricular ejection, and early diastole.

During the late diastolic phase of the cardiac cycle, the aortic and pulmonary (semilunar) valves are closed because the ventricular pressures are lower than either the

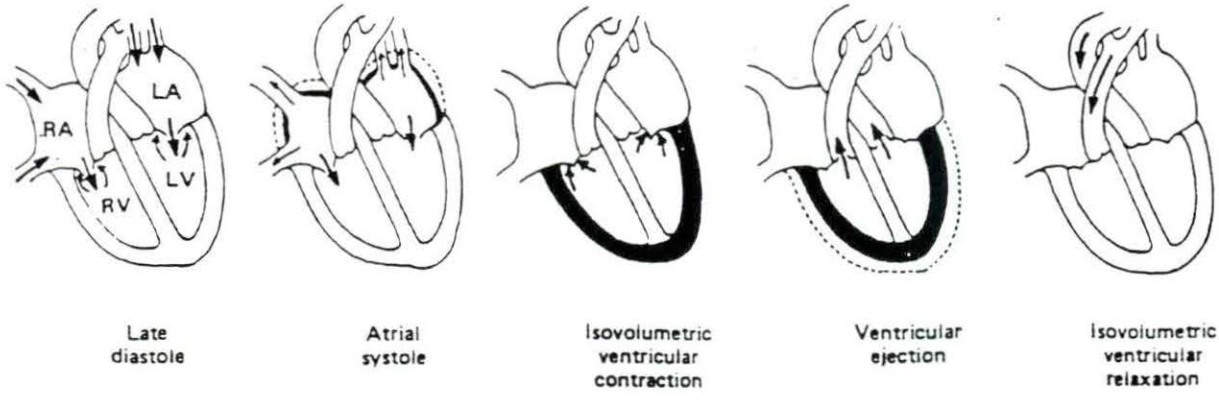

Figure 1.1 : Illustration of the stages of the cardiac cycle (Ganong, 1993).

aortic and pulmonary arteries' pressures. The tricuspid and mitral valves, also called atrio-ventricular valves, are open allowing blood to flow through the heart and to fill the ventricles. The major portion of the coronary circulation takes place during diastole to nourish the heart muscle.

The systolic stage can be divided into two sub-stages: atrial systole and ventricular systole. During atrial systole a small amount of blood is pumped from the atria to the ventricles. However, about 70% of the ventricular filling occurs passively, before atrial contraction, during diastole (Ganong, 1993). Ventricular systole starts prior to atrio-ventricular valve closure. After both the mitral and tricuspid valves close there is a period of isovolumetric contraction, when the pressures in the ventricles increase very fast, and the ventricular volumes remain constant. This rapid increase in intraventricular pressures is due to the contraction of the walls of the ventricles. Intraventricular pressure continues to increase until it exceeds the pressure of the both the aorta and pulmonary arteries. The ventricular pressure value for opening the aortic valve is around 80 mm Hg, and that for opening the pulmonary valve is 10 mm Hg (Ganong, 1993).

The next stage of ventricular systole is called ventricular ejection. Ejection is initiated when both aortic and pulmonary valves are open and the stroke volume of blood is delivered to the circulation during this phase.

Finally, during early diastole, the intraventricular pressure has already begun to decrease. This period of 0.04 seconds is referred to as protodiastole. Since the pressure in the ventricles is now less than the pressure in the arteries, both the aortic and the pulmonary valves close. A period of isovolumetric relaxation is now observed during which the pressure in the ventricles decreases sharply to resting pressure. Early diastole ends when the atrio-ventricular valves open due to the decrease in ventricular pressure below the atrial pressure. The opening of the mitral and tricuspid valves denotes the start of the cardiac cycle again.

From this description it can be observed that an aortic compliance calculation is of great importance at the time of the ventricular ejection phase. It is at this time that the blood enters the aorta from the left ventricle. Because of the high peripheral resistance, or afterload, encountered by the heart at the level of the aorta, blood must be pumped from the left ventricle to the aorta. This factor will induce an increase in pressure which the artery is going to compensate for with an increase in cross-sectional area. For a given ventricular pressure in a normal heart, the higher the afterload is, the shorter the ejection phase will be. In addition, as the peripheral resistance is increasing, the stroke volume will decrease. Following Starling's Law of the Heart, which relates the cardiac output to stroke volume and heart rate, as the stroke volume is decreasing, the heart will maintain its cardiac output by increasing the heart rate or pumping pressure.

As mentioned earlier, aortic compliance refers to the change in cross-sectional area with respect to a change in transmural pressure . The transmural pressure is defined as the pressure difference between the internal and external pressures across the walls of

the aorta. Clinically, changes in aortic compliance can denote several types of heart malfunctions. One of these heart failure diseases is calcification in the arteries which leads to stenosis (stiffening of the arterial walls). Calcification is a process in which there are calcium deposits on the valve leaflets and on other sites in the vessel. As a result, the valve leaflets become hard, and the valve opening becomes too small for the ejection of the blood. This process is referred to as stenosis.

Taking into consideration the importance of the calculation of aortic compliance in the field of medicine, the goals of this study are:

- To design an experiment to obtain ascending aortic diameter values using ultrasound invasively and non-invasively.
- To conduct experiments to acquire complete data sets of both invasively and non-invasively obtained aortic diameter measurements prior to and following hemorrhage.
- To analyze the acquired data to determine the diameter of the ascending aorta when the total blood volume is reduced by thirty percent.

CHAPTER 2: LITERATURE REVIEW

Ultrasound has been studied since the early 1920's. However, the study of the heart using ultrasound, or echocardiography, was not introduced until 1954 by Edler and Hertz in Sweden. Their hypothesis was that sound waves reflected from various structures of the heart within the thorax could be obtained and that this technique would help them study stenosis. In 1961 Edler demonstrated that echoes could actually be obtained from the surfaces of the mitral, tricuspid, and aortic valves (Wells, 1972). Since then the field of ultrasound has grown in popularity in various biomedical fields. Today echocardiography is used extensively in many medical and biological research applications and in therapeutic and diagnostic medicine.

To fully explain this research project it is necessary to discuss the fundamental principles of ultrasound. For this reason, this section will include background information regarding the nature of ultrasound, diagnostic methods of using ultrasound, and essentials of piezoelectricity.

The nature of ultrasound

Ultrasound is a form of energy which consists of mechanical vibrations that produce frequencies which are above the range of human hearing.

Ultrasonic signals travel through any medium in the form of waves. From wave theory, it is known that when sound waves are traveling in a medium of a given density, they will be reflected to their initial source as they encounter an acoustic interface at the

boundary of another material with a different density. The reflection is not complete since there is a part of the wave that penetrates this density boundary and continues into the second medium. This is the basic principle of ultrasound, and it is used in internal medicine and cardiology diagnosis (see Figure 2.1).

The frequency of the sound waves generated for ultrasound studies usually begins at a frequency higher than the greatest frequency audible by the human ear (20 kHz). In cardiology most of the applications employ frequencies in the range of 1-15 MHz.

An external source is needed to produce the vibrations required to transmit the ultrasonic waves into a biological medium,. This source is usually a transducer in the form of a probe. The electrically driven probe is placed in close contact with the surface to be studied. The functioning unit inside the transducer is a piezoelectric (pressure-electric) material, usually a crystal, capable of sending and receiving an ultrasonic signal in pulsed intervals. This piezoelectric crystal vibrates as it is electrically stimulated, and it emits the ultrasonic signals in short pulses (1 microsecond in duration at a rate of 1000 per second). The crystal can convert the ultrasonic echoes returning from the medium into electrical energy which can be displayed using an oscilloscope. The rationale for using pulsed signals in echocardiography is that to use the transducer as a receiving device, signal transmission must occur for a very short time, approximately 1/1000 of each second. Using this process, the transducer can be used as a receiving element.

Diagnostic modes of using ultrasound

The ultrasound technique can be used in many different ways in order to obtain echo information from tissue structures. The following methods have been extensively

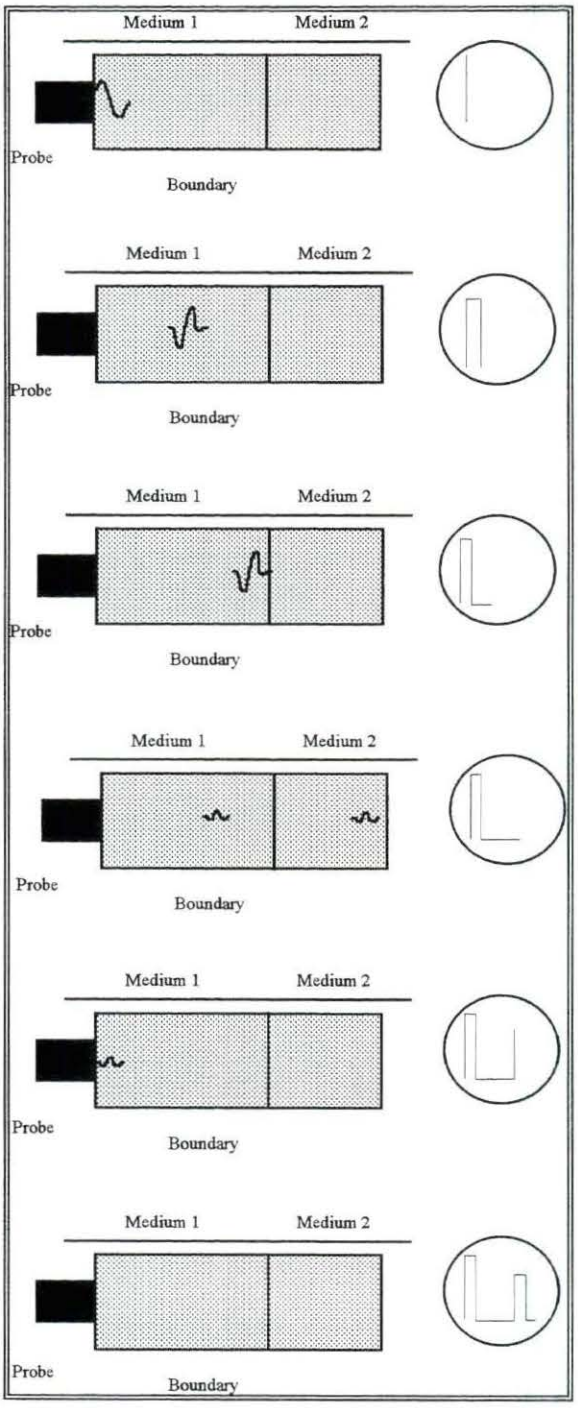

Figure 2.1: Fundamental principle of ultrasound (Wells, 1972).

used in hospitals, and depending on the application, a mode is selected to give the best display of the structures being observed.

The amplitude mode (A-mode)

The amplitude mode, or A-mode, is the simplest technique for ultrasound diagnostics. In this method, the transducer is placed directly over the site where the structure is located, and a single beam is used. The transducer functions as both transmitter and receiver. Compared to other methods, the equipment is simple and inexpensive. The A-mode is a one dimensional recording since it can only detect echoes from body surfaces located along the path of the beam. In the A-mode the returning echoes are displayed as peaks on a horizontal line. The higher the intensity of the returning sound, the higher the amplitude of the peak at that tissue depth (Han and Hurd, 1994) (see figure 2.2).

The amplitude mode can be used advantageously for diagnostic endeavors where the anatomical structures are not complex. It facilitates the study of body interfaces which give rise to echoes. Examples of these structures include the midline of the brain and the bulb of the eye (McDiken, 1976).

The biggest disadvantage of using the A-mode can be seen when complex structures are scanned. The reflected echoes are very difficult to analyze, and it is a very challenging task to interpret the source of these echoes.

The brightness mode (B-mode)

The B-mode, or brightness mode, is a two dimensional scanning method used to facilitate the representation of the tissue structures by ultrasound. During the B-mode, the ultrasound beam sweeps in a plane section through the body. For each beam position

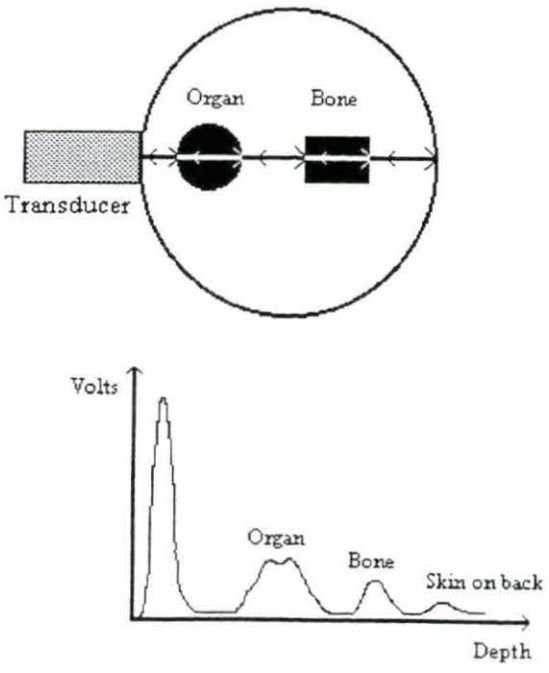

Figure 2.2: Illustration of the amplitude mode in ultrasound. Echoes are displayed as peaks on a graph (Miles, 1989).

surfaces are located by noting the times of the returning echoes and the beam direction (McDiken, 1976). Thus, one advantage of the B-mode over the A-mode is the fact that with the former a two dimensional picture can be obtained from the ultrasound echoes being reflected (see Figure 2.3).

In the B-mode, the brightness increases with the echo amplitude. In this method, the transducer is moved over the area. The echoes reflected from this area will be detected and displayed as dots along the line. As the transducer is moved, the axis of the ultrasonic beam is also moved, and the detected signal will be displayed to correspond with the shifting of the transducer (see Figure 2.4). The echo, shown as dots in the

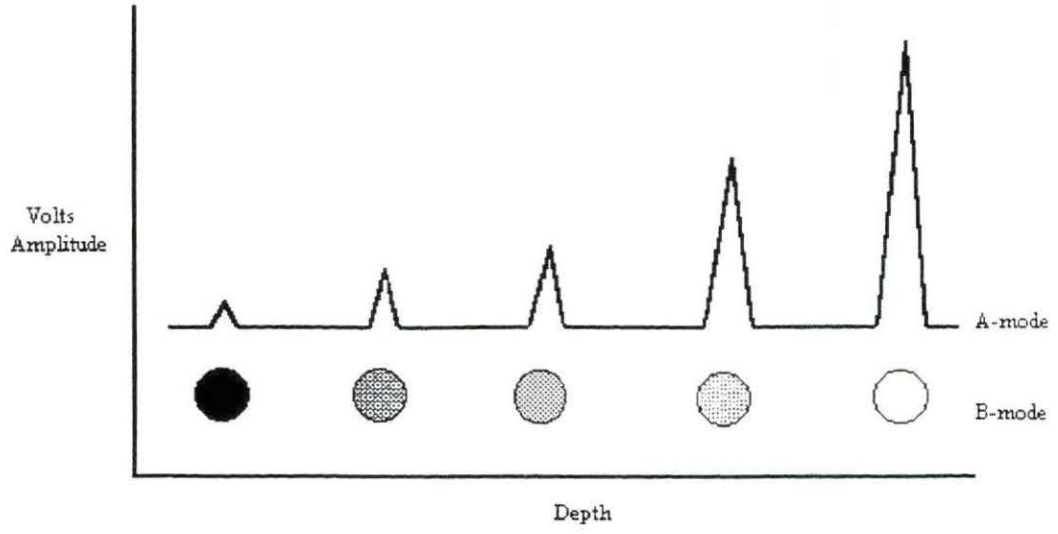

Figure 2.3: While the A- mode uses peaks to depict strength of returning echoes, the B-mode uses bright pixels or dots on a monitor (Han and Hurd, 1994).

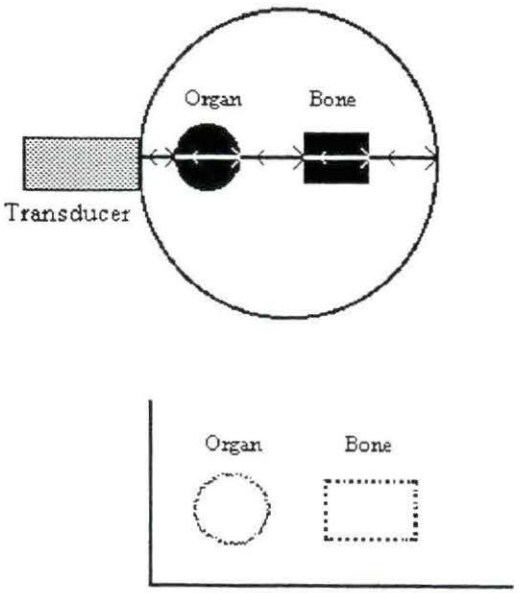

Figure 2.4: Illustration of the brightness mode (B-mode) (Miles, 1989).

screen, forms a two-dimensional image which represents the structures of the body that were analyzed. The dot's degree of brightness is proportional to the intensity of the returning echo; the higher the intensity the brighter the dot (Han and Hurd, 1994).

The motion mode (M-mode)

The M-mode, or motion mode, is the most popular approach used in pulsed ultrasound diagnostics today. As with the A-mode, the M-mode provides a one dimensional view into any tissue structure of the body. The M-mode images represent echoes from various tissue interfaces along the axis of the beam of the transducer (Nelson and Couto, 1986).

The procedure for getting an M-mode uses the same type of scanning as for the A-mode. The transducer beam is held fixed in a plane directed at the tissue of interest. The reflected echoes are swept across time. The recorded display is a representation of the structures in relation to the axis of the transducer at any given point in time.

The value of the motion mode lies in cardiology. However, one limitation of the M-mode is the difficulty of achieving the same beam placement for repeated measurements and calculations. A facility for M-mode, or time-motion scanning, is present on most diagnostic instruments and is of great interest and usefulness in the non-invasive investigation of the heart (see Figure 2.5).

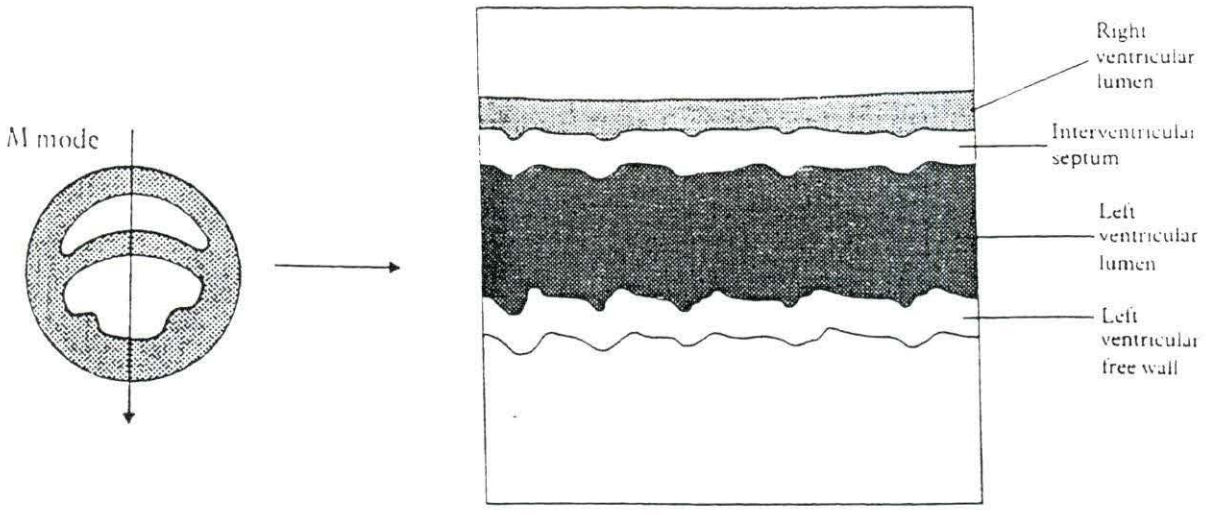

Figure 2.5: Illustration of the motion-mode (M-mode) (Han and Hurd, 1994).

CHAPTER 3: FUNDAMENTALS OF ANATOMY

The anatomy of the dog was studied in this project. A thorough understanding of the structure and function of the ascending aorta and the position of the heart in the dog was required in order to perform all the necessary surgical procedures. The following sections are a review of the microscopic composition of the arteries in the vascular system as well as an overview of the anatomy of the heart of the dog.

Structure and function of the arteries

Anatomy of the aorta

The anatomy of the canine arterial tree including the aorta and its main branches is illustrated diagrammatically in Figure 3.1. The canine aorta has a unique anatomy. It first emanates from the left ventricle at the aortic valve to give rise to the ascending aorta. This region is very short and is the primary section of interest in this study. The ascending aorta is the origin of arteries branching to the heart, head, and upper limbs. The aorta turns 180° and continues as the descending aorta. The first part of the descending aorta, before it passes through the diaphragm, is called the thoracic aorta. After penetrating the diaphragm, the thoracic aorta becomes the abdominal aorta. In this region it gives rise to arteries supplying blood to all the abdominal organs. As the abdominal aorta continues, it branches to form the iliac vessels which deliver oxygenated blood to the hind limbs.

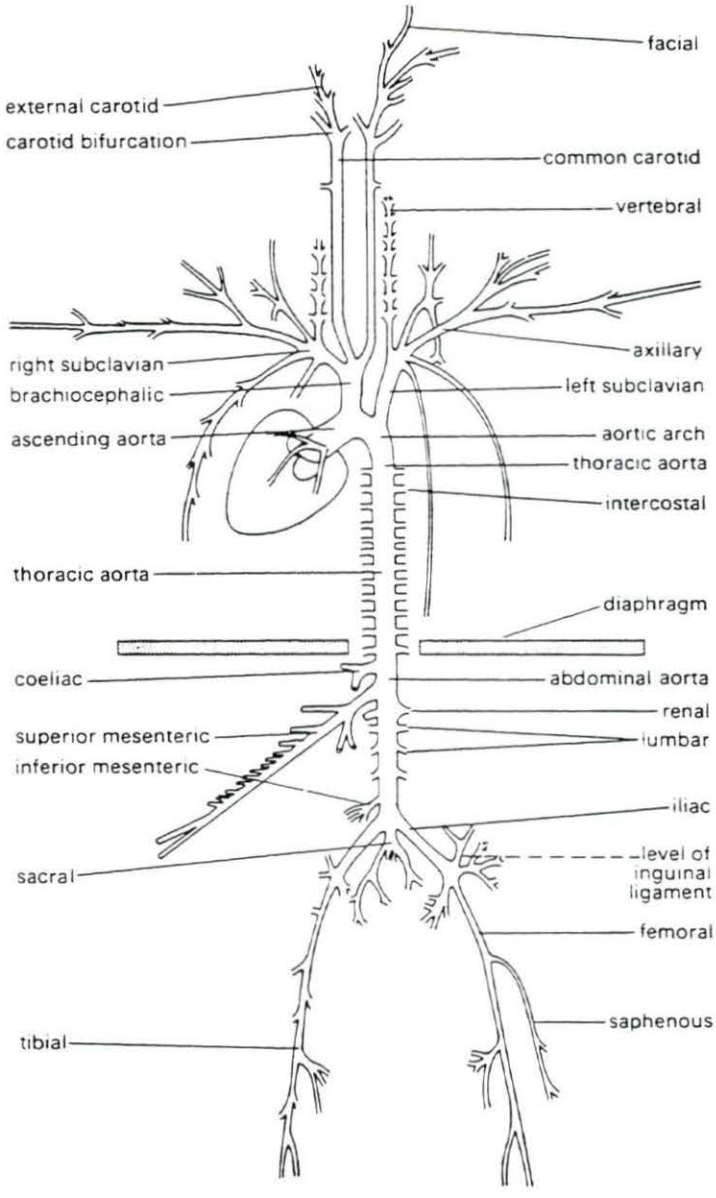

Figure 3.1: A diagrammatic representation of the major branches of the canine arterial tree (Caro, Pedley, Schroter, and Seed, 1978).

Microscopic structure of the arterial wall

The wall of the arteries (and the veins), except for the vessels of the terminal circulation, are composed of three distinct layers: an innermost layer called *tunica intima*, a middle layer called *tunica media*, and an outermost layer called *tunica adventitia*. Furthermore, there exist significant differences in the cell composition and structure of each of these layers within the vessels. This differentiation is mostly in response to the different mechanical demands made on the specific vessels and their special functions in different parts of the body.

The first, innermost layer of the arterial wall can be subdivided in three essential elements for ease of discussion: the *endothelium*, the *subendothelial layer*, and the *internal elastic lamina*.

The *endothelium* serves as a lining throughout the circulation. It consists of a single layer of cells that cover all the elements that are in contact with the blood (arteries, capillaries, veins, and heart valves as well as all the other endocardial surfaces). The *endothelium* is a very delicate layer and high pressure or high shear stress can damage it. On the other hand, its capacity to regenerate is very high. The *endothelium* constantly regenerates itself and can grow to form a lining over synthetic vascular graft materials and artificial heart valves.

Surrounding the *endothelium* there is a layer composed of many fibroblasts, or collagen-generating cells, called the *subendothelial layer*. This cover is very strong because of the presence of collagen fibers and serves as a protective element for the inner layer. It is in close contact with the *internal elastic lamina*.

The *internal elastic lamina* is the last component of the *tunica intima* and is composed of elastic fibers that gives the artery its elastic properties. This layer is very

well defined in smaller arteries. Moreover, under microscopic analysis, the *internal elastic lamina* marks the inner boundary of the *tunica media*.

The *tunica media* is the thickest layer in the wall of the arteries and depending on the region of the circulation being studied, this layer varies in structure and properties. In the aorta and its main branches within the chest, the *tunica media* consists of several layers of elastic tissue separated by collagen fibers, thin fibers of connective tissue and very little vascular smooth muscle which cross-links the elastic layers. This layered structure of the *tunica media* in the arteries is often referred to as *lamellar* structure. Moreover, these *lamellae* have a fairly constant thickness of about 15 μm, so that the total number present is closely proportional to the radius of the vessel both between and within species (Caro, Pedley, Schroter, and Seed, 1978).

The structure of the *tunica media* will change in the vessels further from the heart. Elastic fibers will be less prominent in the vessels in the periphery. In this area the *tunica media* will consist mostly of spirally arranged vascular smooth muscle layers with very little connective tissue, collagen, and elastic fibers. However, the *tunica media* of smaller arteries will become the predominant element in their walls. This region will be separated from the *tunica adventitia* by an thin layer of elastic tissue known as the *external elastic lamina* (Caro, Pedley, Schroter, and Seed, 1978).

Finally, the third and outermost arterial wall layer is the *tunica adventitia*, also referred to as *tunica externa*. This layer is mostly composed of loose connective tissue with little elastin and collagen fibers. An important point to mention is that the *tunica adventitia* ensures that the arteries are built into their surroundings in a functionally correct manner. Consequently, the *tunica adventitia* merges with the surrounding tissues and its outer limit is not obvious.

Based on the microscopic structure of the arterial wall, it is clearly seen that the arteries can be mainly classified by the composition of their *tunica media*. The following section will describe the two types of arteries: the elastic arteries and the muscular arteries.

Classification of the arteries

The arteries can be classified into two distinct types based on their microscopic structures, the elastic arteries and the muscular arteries. The elastic arteries include the vessels that function near the heart. Basically, the elastic arteries include the aorta and its branches and the pulmonary trunk. These vessels are yellow in appearance because of the presence of elastin in the *tunica media*. In the elastic arteries, the *lamina elastica interna* will combine with the other elastic membranes and form the structure of the *tunica media*. The tension on the arterial wall is regulated by muscle cells linked to elastic structures called *elastic lamellae*.

The significance of the tunica media of the elastic arteries in the vascular circulation can be best described using the aortic circulation as an example. During systole, the blood which has been pumped into the aorta puts the *tunica media* under elastic tension. Some of the power produced by the heart as it is beating is temporarily retained as potential energy. Furthermore, during the diastolic phase this energy is changed to kinetic energy by the recoil of the vessel wall. This way the blood expelled from the heart in rhythmic strokes is transported to the periphery in a much more even stream. The function of the aorta, and the other arteries of elastic types, can be compared with that of an expansion compartment (Nickel, Schummer, and Seiferle, 1981).

Moving to the periphery, the elastic arteries merge into the muscular arteries. The muscular arteries are reddish or white in color and have a very thick wall. As the name implies, these arteries have vast amounts of vascular smooth muscle present in the media layer (Nickel, Schummer, and Seiferle, 1981). Moreover, the muscular arteries serve as distributing systems throughout the body. Their function is to carry the blood to their target organs. As they do so, the pressure of the blood will have a stretching effect on their walls in both the longitudinal and circular directions.

To better understand how the muscular arteries compensate for these pressure changes, it is important to recall the internal structure of the blood vessels, specifically the composition of the *tunica media* and the *tunica adventitia*. As mentioned earlier, the *tunica media* in muscular arteries is largely composed of vascular smooth muscle arranged in a spiral fashion. The *tunica media* can overcome the transverse tension changes by either constricting or by allowing the pressure to dialate the lumen of the vessel. Therefore, this will regulate the blood pressure within the arterial system and maintain it within physiological limits. Moreover, the *tunica adventitia* will compensate for the longitudinal tension changes since it is composed of little collagen and elastic fibers which are arranged in a cross helical fashion (Nickel, Schummer, and Seiferle, 1981).

Anatomy of the heart in the dog

The position of the heart within the thorax corresponds to the wedge shaped sternum which is bilaterally flattened. In the dog the long axis of the heart forms an angle of 40°, open anteriorly, with the sternum. The base of the heart lies at the level of

an imaginary horizontal plane, drawn through the center of the first rib. The anatomy of the heart is shown in Figure 3.2.

Unlike the heart of a man, which is entirely accessible for clinical examination by auscultation from the thoracic wall, in domestic mammals this organ does not lend itself to these procedures. In the dog the anterior part of the thorax, which accommodates the heart, is covered by extensive shoulder girdle musculature, which is connected to the shoulder blade and the humerous, and by the massive biceps brachii muscle which fills the angle between these two bones (Nickel, Schummer, and Seiferle, 1981).

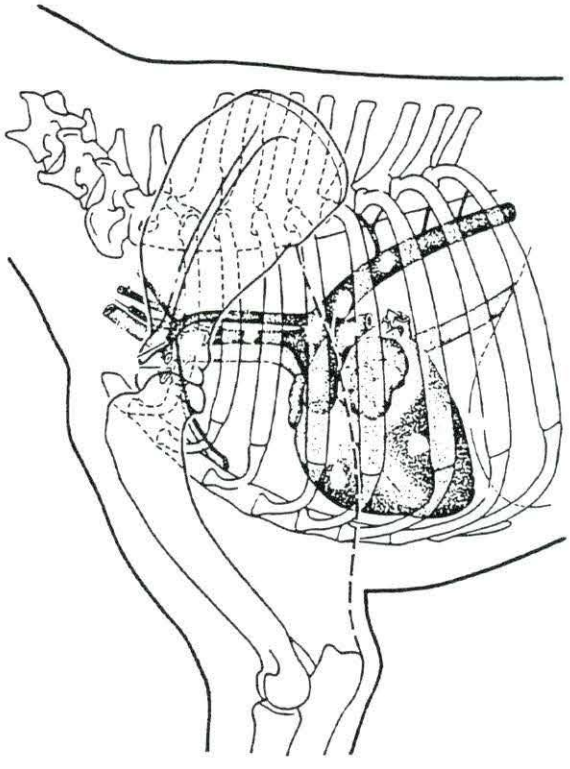

Figure 3.2: Anatomy of the heart of the dog (Nickel, Schummer, and Seiferle, 1981).

CHAPTER 4: MATERIALS AND METHODS

This research project was divided into three experiments. In every experiment non-invasive and invasive measurements were taken using the ultrasound workstation. The non-invasive measurements were taken with the subject placed in left lateral recumbency and the transducer placed in the intercostal space between the fourth and fifth ribs. Furthermore, the invasive measurements were taken following the thoracotomy. For these recordings the transducer was placed directly on top of the ascending aorta while the heart was beating.

The first experiment, which included three dogs, was a study of the sensitivity of the ultrasound workstation. In the second experiment the aortic diameter changes were studied in two dogs while the subject was undergoing hemorrhage, prior to the invasive technique. The third experiment included two animals in which hemorrhage was induced after the thoracotomy was performed. Using these experimental methods, non-invasively derived aortic diameter measurements were compared to invasively derived aortic diameter measurements at several different levels of aortic pressure.

This section of the report includes an explanation of the experimental designs and surgical protocols.

Experimental design

The dogs used for these experiments were between the ages of 3 and 5 years. All the dogs were in good physical condition, without parasites or heart worms. They were not fed the day before the experiment.

Experiment 1: Sensitivity study

The sensitivity study was designed to test the accuracy of the ultrasound workstation. For this part of the research, three dogs were studied. Measurements of the aortic diameter during the systolic and diastolic phases of the cardiac cycle were taken. By taking repeated measurements of the aortic diameter prior to and following thoracotomy, the linearity and reliability of the equipment used for this project were determined.

Two scan positions were of interest. First, a short-axis view depicting the aorta in cross-section was obtained by placing the transducer between the fourth and fifth ribs on the dog during the close chested scans and directly against the aorta in the open chested scans. This short axis view was required for M-mode application and was ultimately used in diameter measurements.

Second, an apical long-axis view, depicting the apex of the heart at the top of the scan and the aortic flow pointing toward the bottom of the image (see Figure 4.1) was obtained. This view is acquired by placing the transducer below the ribcage, and it is required for Doppler flow measurements. For accurate results, correct transducer orientation is crucial in order to depict aortic flow in this vertical direction. The scan depth was varied in order to achieve the maximum resolution of all images.

M-mode data, which yields a real time analysis of the ultrasound scan at one line in the two-dimensional image, was then analyzed on the Interspec Cardiology Workstation (refer to Appendix A for specifications). The desired image was frozen on the screen and calibrated. The length measurements were taken at selected points both in the two-dimensional scan and M-mode view. Adopting American Medical Association standards for echocardiography, distances were measured by applying the

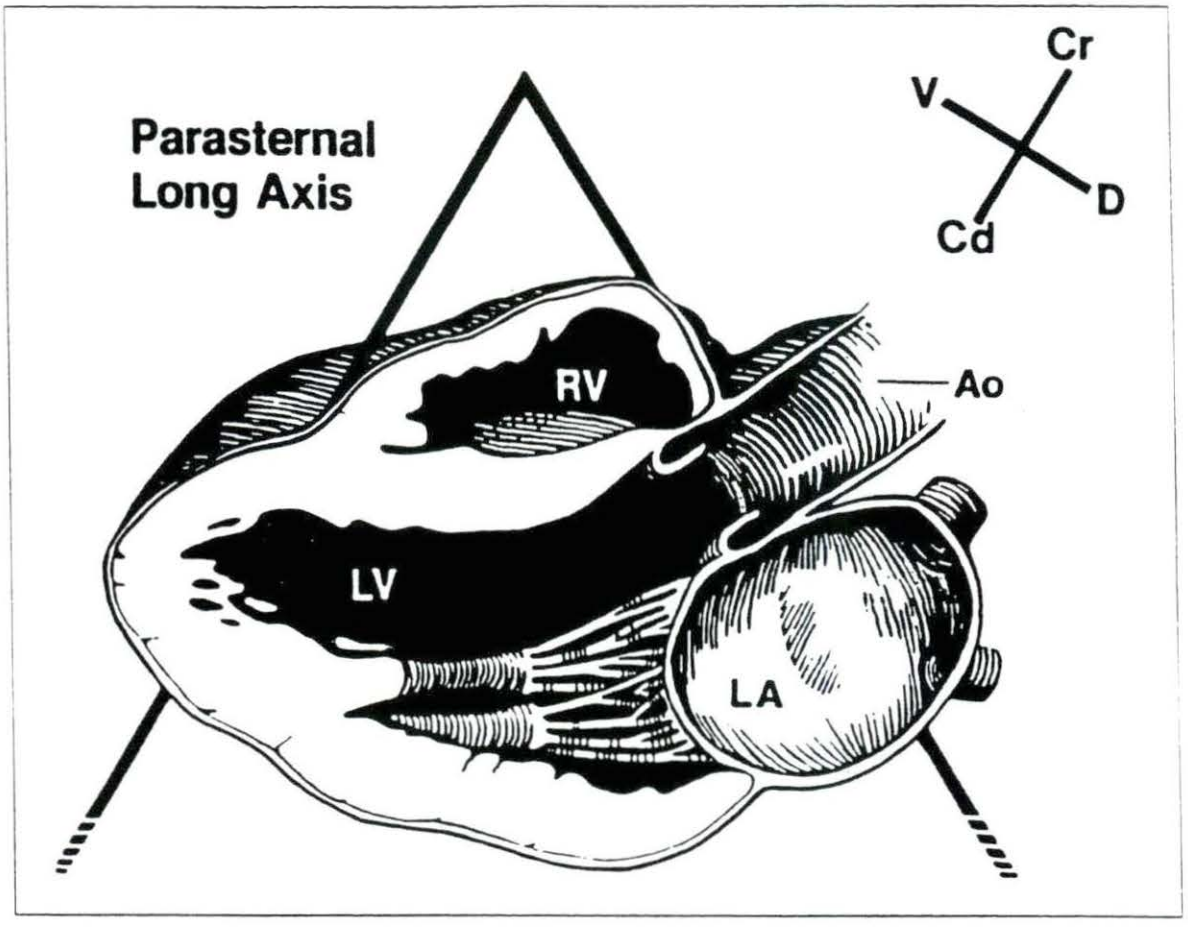

Figure 4.1: Cross-sectional anatomy of the heart displayed in a long axis projection (Miles, 1989).

"leading edge to leading edge" technique. This method involved including the top aortic wall thickness (as represented in the M-mode image) in the length measurement and excluding the bottom aortic wall thickness in order to incorporate one wall thickness into the diameter measurement (see Figure 4.2).

For each image analyzed, several systolic and diastolic diameter measurements were taken. Several positions during systole and diastole were located on the M-mode image by noting valve leaflet position. From the two dimensional images, a completely closed aortic semilunar valve indicated the diastolic phase, while a completely open valve indicated the systolic phase of the cardiac cycle. In addition the systolic and diastolic phases were correlated with an electrocardiogram taken simultaneously throughout the experiment. M-mode diameter readings were also compared to those images taken from the two-dimensional scan.

Prior to thoracotomy, measurements of the aortic diameter were taken after the subject was sedated with Xylazine (0.2 mg/kg)-Butorphenol (0.2 mg/kg) -Glycopyrrulate (0.005 mg/kg) tranquilizer (XBG). This sedative works well with dogs and has a slight effect on the heart rate (Miles, 1989).

During the preparation for the thoracotomy, the animals were anesthetized with sodium pentobarbital (15 mg/kg). Lungs were ventilated by means of a respirator with room air (Harvard Respirator Pump) to maintain oxygenation. Following exposure of the heart, the transducer was placed at the aortic root and supra-aortic ridge (above the apex of the valve commissures). Positioning at this specific site is necessary for the compliance measurement because this is the position of the unstented heart valve placement which is a concern to the FDA. Objects directly against the transducer cannot be read accurately, thus a spacer was attached to the transducer to maintain resolution.

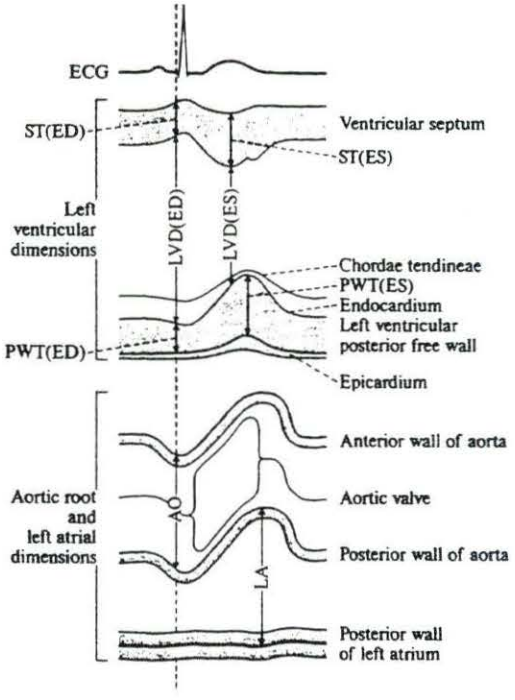

LVD(ED) Left ventricular internal dimension at end-diastole measured at onset of QRS complex

LVD(ES) Left ventricular internal dimension at end-systole measured at peak posterior motion of ventricular septum (corresponds to minimum internal dimension)

ST(ED) Ventricular septal thickness at end-diastole measured at onset of QRS complex

ST(ES) Ventricular septal thickness at end-systole measured at maximum thickness [not included in ASE recommendations]

PWT(ED) Left ventricular posterior free wall thickness at end-diastole measured at onset of QRS complex

PWT(ES) Left ventricular posterior free wall thickness at end-systole measured at maximum thickness [not included in ASE recommendations]

AO-'ASE' Aortic root dimension at end-diastole measured at onset of QRS complex from leading edge of anterior wall of aorta to leading edge of posterior wall of aorta

LA-'ASE' Left atrial dimension at end-systole measured at the maximum dimension from the leading edge of the posterior wall of aorta to the dominant line representing the posterior wall of the left atrium (identified by the switched-gain circuit or by manual damping)

Figure 4.2: American Medical Association standards for echocardiography (Berne and Levy, 1990)

The spacer is a condom filled with conductive gel. An electrocardiogram was recorded in order to correlate systolic and diastolic phases during the M-mode measurements.

Using both the Motion mode (M-mode) and the 2-dimensional view, four different measurements of aortic diameter were taken in the sensitivity study: systolic phase, diastolic phase prior to thoracotomy and systolic phase and diastolic phase following thoracotomy. These measurements were made using the "leading edge technique" explained earlier in this chapter.

On the M-mode image, the aorta appears as two parallel lines undulating upward in systole. During diastole, one or two aortic valve cusps may be seen as a straight line parallel to and in the center of the aortic wall echoes (see Figure 4.2). At the onset of the ejection (systolic phase) the cusps quickly separate to opposite sides of the aortic root, then come together again at the end of ejection (diastolic phase).

The diameter of the aorta is determined at the end of diastole. For this reason, the diastolic measurements taken throughout the experiment were analyzed and then compared to the mechanical measurement recorded following euthanasia of the subject.

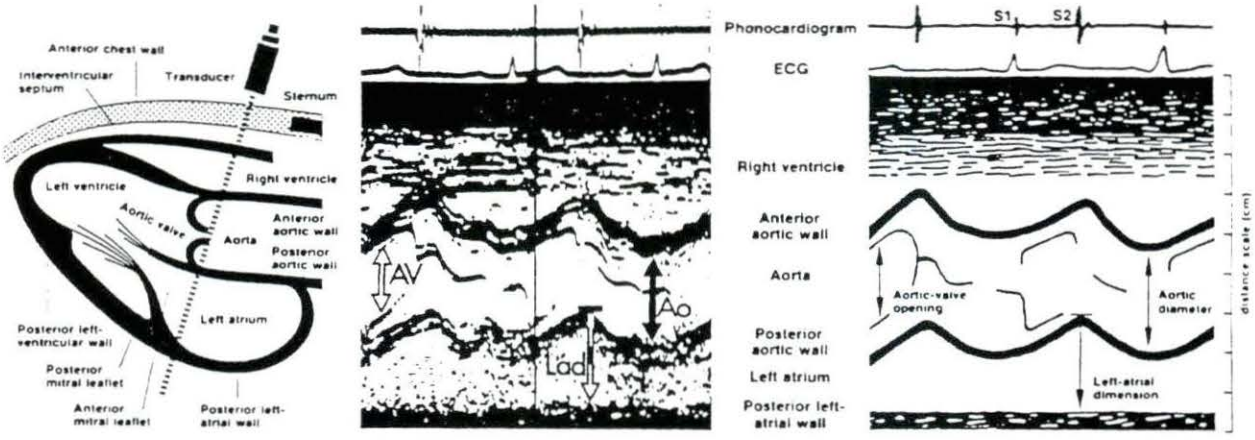

Figure 4.3: With the ultrasound beam at this angle, the aortic root, aortic valve opening and the left atrium are visualized (Termini and Lee, 1976).

In addition, systolic diameter measurements were collected to show variability and linearity of echocardiographic calculations in the cardiac cycle.

The ultrasound equipment can directly record the diameter as well as blood flow and velocity values. It digitizes an analog signal and is capable of producing multiple readouts. The echo can be read on the monitor or transferred to a computer screen. In this project, the measurements were printed on thermal paper and stored on VHS tape.

Experiment 2: Hemorrhage induced prior to thoracotomy

This experiment was designed to study the behavior of the diameter of the ascending aorta when thirty per cent of the total blood volume was taken from the subject in a period of fifteen minutes. The hemorrhage was induced prior to the thoracotomy.

As the subject is losing blood the pressure in the vascular system decreases. The body will tend to compensate for this decrease by changing the resistance in the muscular arteries in the periphery of the body. Consequently, the vascular smooth muscle of the arteries will contract in a process called vasoconstriction. From this process, more blood will flow through the vital organs (heart, kidneys, and brain) and less blood will flow through the periphery.

As mentioned in Chapter 3, the aorta and the pulmonary arteries are classified as elastic vessels in the cardiovascular system. This is because of their high content of elastic fibers. The diameter of the aorta will not change during vasoconstriction because of the relative lack of smooth muscle fibers. Moreover, as the blood volume and pressure are rapidly changing because of the hemorrhage, there will be less distention of the elastic fibers in the ascending aorta. As a result, the diameter will begin to decrease.

In order to perform this experiment some variations from the previous experimental protocol were needed. Pressure recordings were required to correlate the diameter decrease with the corresponding pressure change. Aortic pressure was measured invasively, through a femoral artery cannula, with a pressure transducer connected to a Beckman analog recorder. Pressure recordings were taken at several times during the experiment following each hemorrhagic period The transducer was calibrated before it was placed for recording by inflating a balloon to a known pressure read by a sphygmomanometer (see Figure 4.3).

Prior to the non-invasive recordings, the dog was sedated with XBG tranquilizer (1 ml/40 lb), and, before the thoracotomy and invasive recordings, the dog was anesthetized with sodium pentobarbital (15 mg/kg)

Using the 9.5% of the body weight estimation formula, the total blood volume (TBV) was estimated for each subject. From this value, the amount corresponding to a fifteen percent reduction of the total blood volume and a thirty percent reduction of the total blood volume were determined. This amount was then collected using a large cannula in the femoral artery.

Blood pressure and ascending aortic diameter measurements were taken at four different stages during the experiment: control, after 15% total blood volume (TBV) decrease, after 30% TBV decrease but prior to thoracotomy, and following thoracotomy.

Experiment 3: Hemorrhage induced after thoracotomy

In this last two dogs, the behavior of the aortic diameter was studied when the hemorrhage was induced after the thoracotomy. Control recordings of aortic diameter

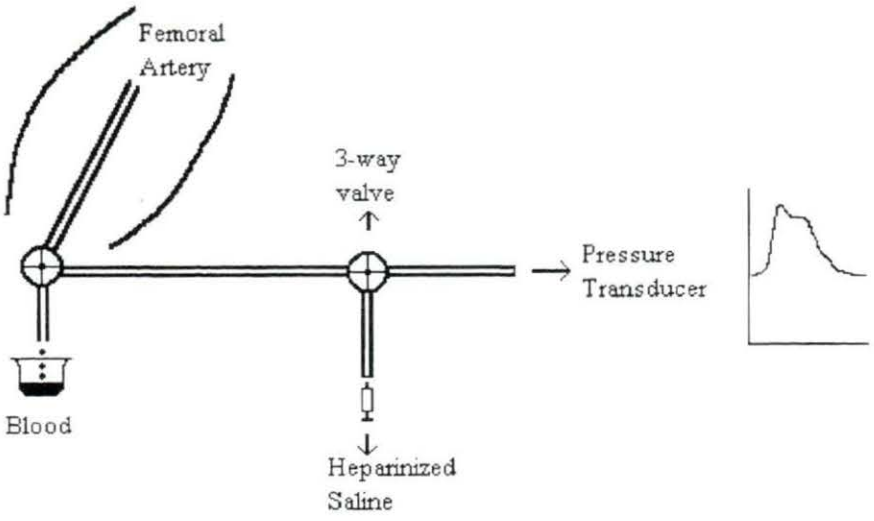

Figure 4.4: Illustration of the procedure for measuring pressure and collecting blood.

were taken, then the subject was intubated and the thoracotomy was performed. Images were again collected and a set of control recordings following thoracotomy were taken.

Once these measurements were made, the subjects were canulated and fifteen percent of the total blood volume was removed (see Figure 4.3). Recordings of the aortic diameter after the first hemorrhagic period were taken and compared with the control values. Fifteen minutes after the first hemorrhage was induced, the animal was bled again until thirty percent of the total blood volume was removed. Aortic diameter was again monitored with the ultrasound workstation. The values were compared with the mechanical value recorded with a caliper after euthanasia of the animal.

CHAPTER 5: RESULTS

This chapter has the results of the three experiments. All data tables, and ultrasound images are in the corresponding appendices B-H.

Experiment 1: Sensitivity study

The sensitivity study used three dogs to test the accuracy of the ultrasound workstation. Table 5.1 summarizes the results for this experiment.

Mean aortic diameter measurements are listed for both the M-mode view and the 2-dimensional view. The mean mechanical measurement for this experiment was 1.71 cm. This value represents one measurement from each subject following euthanasia. Non-invasive diastolic diameter gave an estimated error of 15.78% in the M-mode view and 12.28% in the 2-dimensional view. Furthermore, the smallest errors were found in the 2-dimensional view invasive systolic diameter, 2.92%, and the non-invasive systolic diameter, 3.50%. The percent errors were calculated by the following equation:

$$\{[\mathbf{X}_{(theo)} - \mathbf{X}_{(calc)}] \div \mathbf{X}_{(theo)}\} \times 100 \qquad (5.1)$$

where $\mathbf{X}_{(theo)}$ is the theoretical value and $\mathbf{X}_{(calc)}$ is the calculated value. The theoretical value was assumed to be the mechanical measurement for the diastolic phase. For the systolic phase this estimate was taken from the aortic root diameter values listed in the literature (Nelson and Couto, 1986). There have been several reports of normal reference ranges for echocardiographic measurements in dogs. These values are greatly

Table 5.1: Aortic diameter mean values for the sensitivity study (Dogs #1, 2 ,3)

Type of Measurement	M-mode view (cm)	% Difference M-mode view	2-dimensional view (cm)	% Difference 2-dimensional view	Mechanical measurement (cm)
Systole, prior to thoracotomy	1.9	11.11	1.8	3.50	1.71
Systole, following thoracotomy	1.8	8.77	1.7	2.92	
Diastole, prior to thoracotomy	2.0	15.78	1.9	12.28	1.71
Diastole, following thoracotomy	1.9	11.11	1.6	6.43	

affected by body size (see Table 5.2). The calculated value was the measured value (from the ultrasound images) for both systolic and diastolic diameters.

A factor to consider when analyzing these results is the weight of the animal. Dog #1 weighed 49 lb, dog #2 weighed 41 lb, and dog #3 weighed 27 lb. Diameter measurements could have varied a small amount because the weight of the third animal was not within the same range as the first two dogs.

Figures 5.1 and 5.2 show some of the measurements taken with the M-mode along with the respective diameter calculations. Figures 5.3 and 5.4 illustrate the measurements of the diameter using the 2-dimensional scan.

Table 5.2: Normal canine echocardiographic values for Aortic Root (Nelson and Couto, 1986)

Wt (Kg)	**5**	**10**	**15**	**20**	**25**	**30**	**35**	**40**	**50**
Ao (mm)	15.3 (3.0)	18.1 (2.0)	20.4 (1.4)	22.8 (1.3)	24.6 (1.6)	26.4 (2.2)	28.3 (2.9)	30.0 (3.5)	33.1 (4.8)

Ao= Aortic Root ±SD in parenthesis below

Experiment 2: Hemorrhage induced prior to thoracotomy

Table 5.3 shows the results for the two animals studied in this experiment. For this experiment four different phases were studied: control values prior to hemorrhage and thoracotomy, values following fifteen percent total blood volume decrease but prior to thoracotomy, values following thirty percent total blood volume decrease but prior to thoracotomy, and values following thirty percent total blood volume decrease and thoracotomy.

Table 5.3: Aortic diameter mean values for experiment #2 (Dogs #4, #5)

Type of Measurement	M-mode view (cm)	2-dimensional view (cm)	Pressure (mm Hg)	Mechanical measurement (cm)	Heart Rate (BPM)
A. Control values prior to hemorrhage and thoracotomy					
Systole	1.5	1.5	Mean = 96	1.16 (± 0.007)	125
Diastole	1.7	1.5	130/80		
B. Values following 15% total blood volume decrease, but prior to thoracotomy					
Systole	1.4	1.3	Mean = 83	1.16 (± 0.007)	130
Diastole	1.5	1.3	100/75		
C. Values following 30% total blood volume decrease, but prior to thoracotomy					
Systole	1.3	1.1	Mean = 46	1.16 (± 0.007)	132
Diastole	1.3	1.2	60/40		
D. Values following 30% total blood volume decrease and thoracotomy					
Systole	1.1	1.2	Mean = 56	1.16 (± 0.007)	149
Diastole	1.2	1.2	90/40		

Note: (± SD)

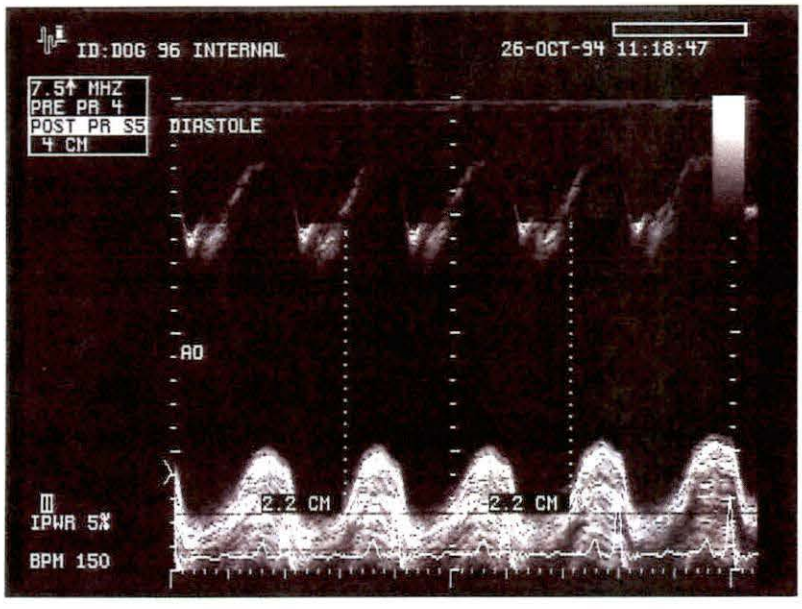

Figure 5.1: M-mode image during diastole (Dog #2 , after thoracotomy).

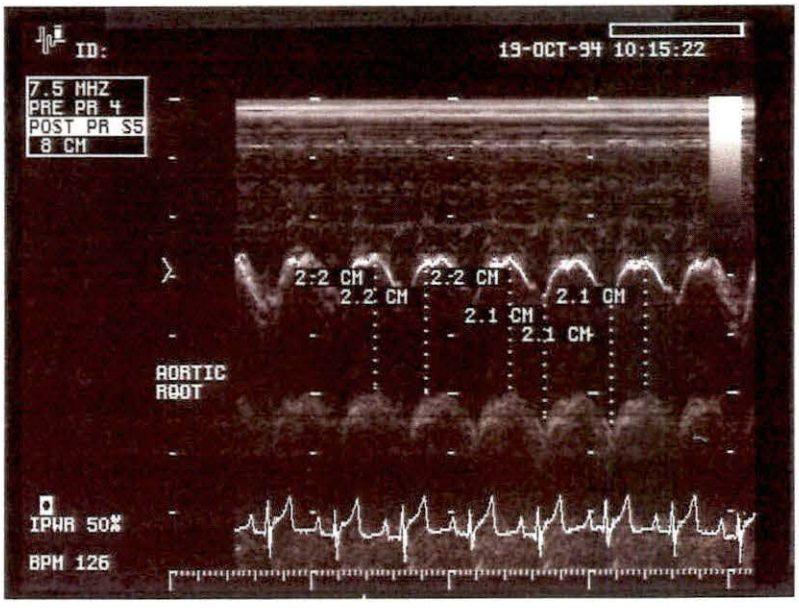

Figure 5.2: Illustration of the M-mode view of the ascending aorta (Dog #1).

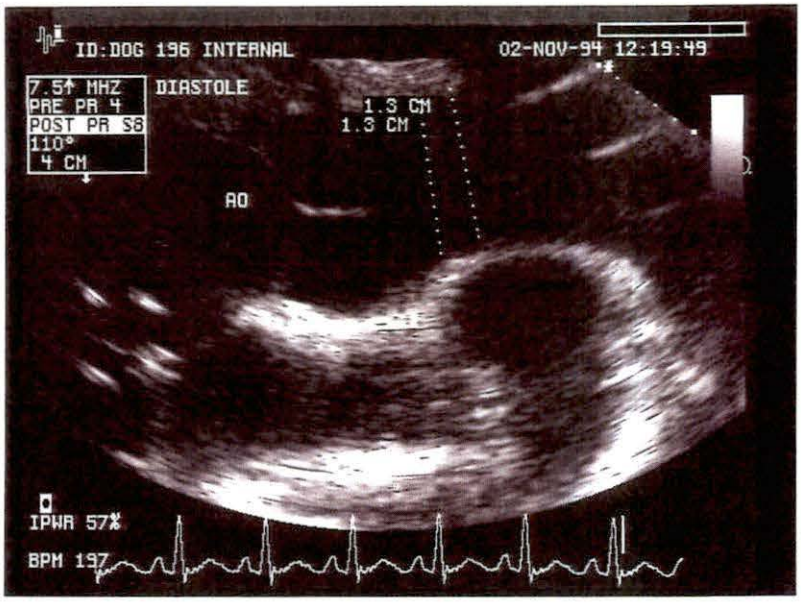

Figure 5.3: Two-dimensional image during diastole. The closed aortic valve can be seen in the image (Dog #3, after thoracotomy).

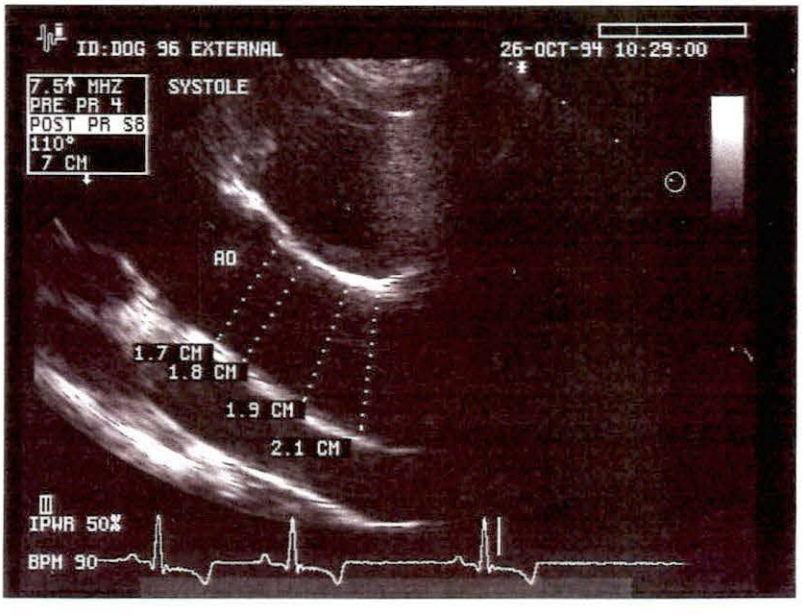

Figure 5.4: Two-dimensional image of the ascending aorta during systole (Dog #2, prior to thoracotomy).

Table 5.3 lists both systolic and diastolic aortic diameter values for the M-mode and the 2-dimensional views. Both dogs weighed 27 lb and 0.68 ml of XBG sedative, a combination of Xylazine (0.2 mg/kg), Butorphenol (0.2 mg/kg), and Glycopyrrulate (0.005 mg/kg), were administered intravenously at the start of the procedure. Control recordings were taken with the subjects in left lateral recumbency, following the same procedure used in the sensitivity study. Images of the aortic root were taken with the M-mode (see Figure 5.5 and 5.6) and the 2-dimensional view (see Figure 5.7 and 5.8). The systolic pressure was recorded to be 130 mm Hg and the diastolic pressure was 80 mm Hg. A mean pressure of 96 mm Hg was calculated during this part of the experiment.

For dogs of 12-15 Kg, a mean diameter of 1.7 cm is given (Nelson and Couto, 1986); therefore the diastolic value from the M-mode view given in Table 5.3 is within the range of normal values of canine ascending aortic diameter based on the weight of the dog. As can be seen in Table 5.3, the mean value of the control diastolic diameter images was 1.7 cm in the M-mode and 1.5 cm in the 2-dimensional scan.. However, for systole the M-mode view produced a systolic diameter of 1.5 cm and the 2-dimensional view produced a value of 1.5 cm.

After taking the control measurements of the aortic diameter, sodium pentobarbital (15 mg/kg) was administered to anesthetize the subject and the femoral artery was canulated. Following this procedure, fifteen percent of the total blood volume was withdrawn from each dog. For dogs #4 and #5, this amount was 175 ml.

The pressure transducer was placed and subsequently blood pressure was constantly monitored. After calibrating the transducer, pressure measurements were taken at all times during the experiment. Once the blood was collected, the next step was to begin recording the pressure changes associated with the loss of blood.

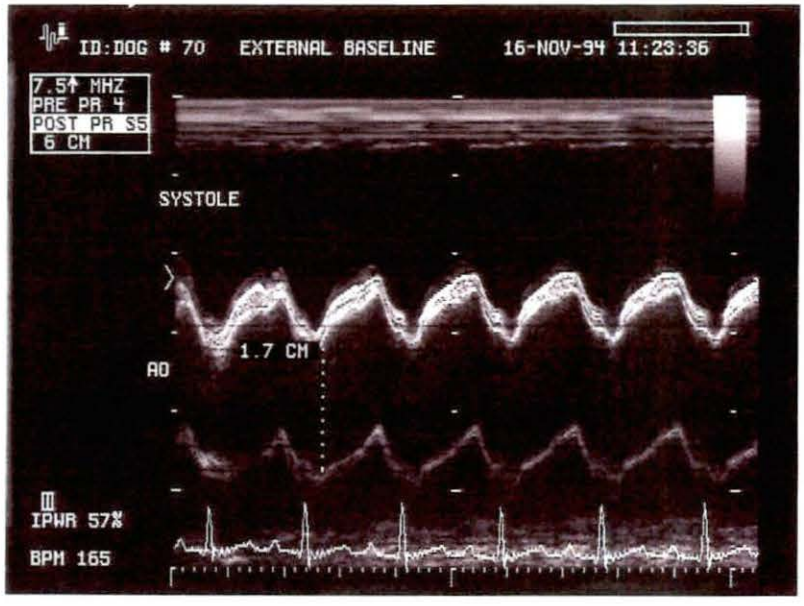

Figure 5.5: M-mode image taken during systole for control values during experiment #2 (Dog #4).

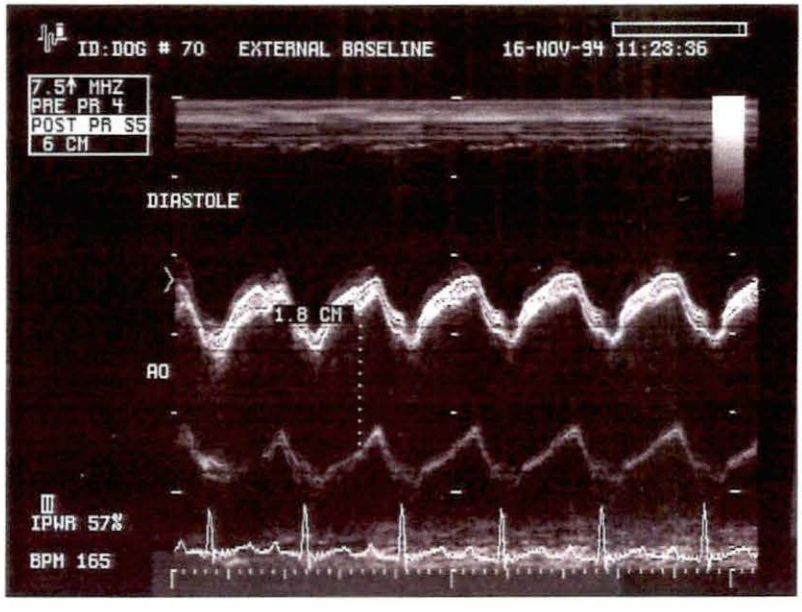

Figure 5.6: M-mode image taken during diastole for control values during experiment #2 (Dog #4).

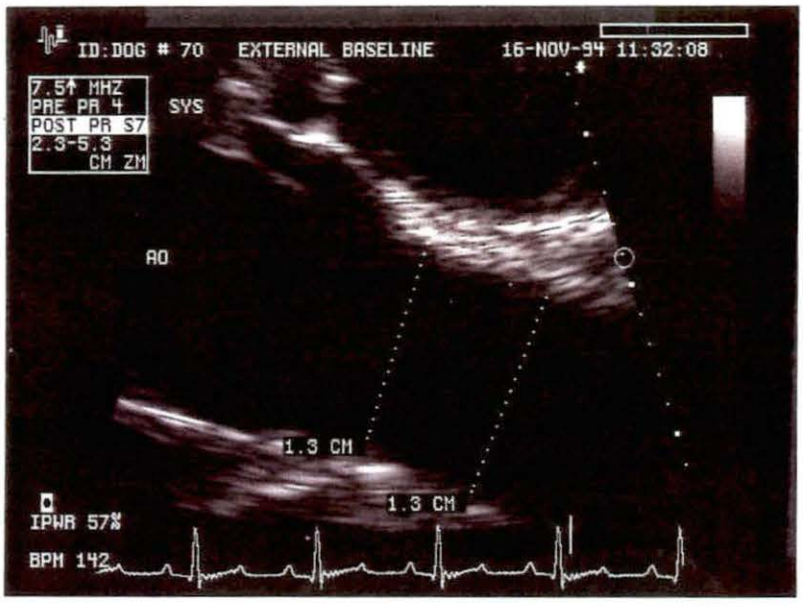

Figure 5.7: Two-dimensional image taken during systole for the control measurements of experiment #2. The zoom function was used for this image (Dog #4).

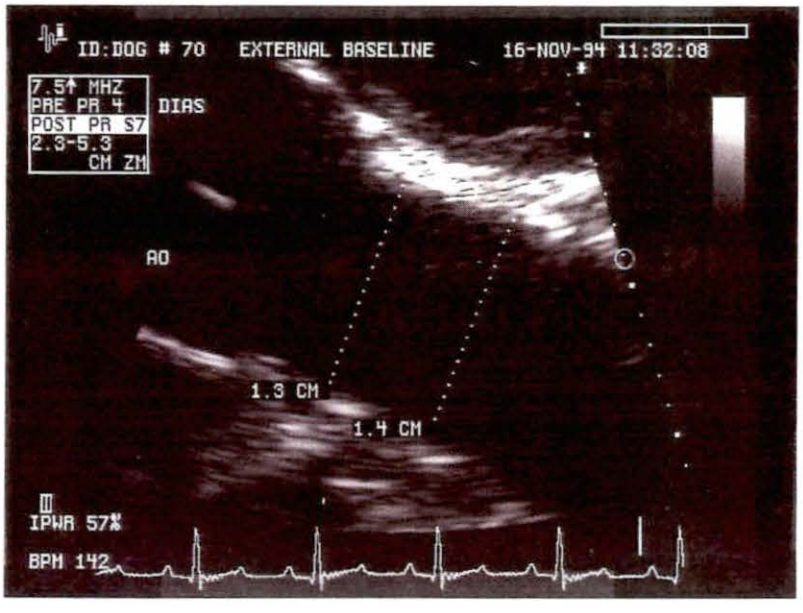

Figure 5.8: Two-dimensional image taken during diastole for the control measurements of experiment #2. The zoom function was used for this image (Dog #4).

The mean arterial pressure, **Pm**, was calculated using the following equation (Bern and Levy, 1990):

$$\mathbf{Pm} \approx \mathbf{P(dias)} + \{1/3 \times [\mathbf{P(sys)} - \mathbf{P(dias)}]\} \quad (5.2)$$

In this equation, **P(dias)** is the diastolic pressure recorded by the transducer and **P(sys)** represents the systolic pressure. Note that his difference is the pulse pressure of the subject.

Following the 15% total blood volume decrease, a decrease in both the systolic and diastolic aortic diameter measurements using the M-mode were recorded, from 1.5 cm to 1.4 cm in systole, and from 1.7 cm to 1.5 cm in diastole (see Figure 5.9 and 5.10). This represent approximately a 11.8% and 6.7% decrease in diastolic and systolic aortic diameter, respectively. The 2-dimensional images also showed that the diameter decreased significantly, from 1.5 cm to 1.3 cm in systole. This depict a decrease of 13.3%. Diastolic diameter values were reduced from 1.5 cm to 1.4 cm, a 6.7% decrease after the removal of the first 175 ml of blood (see Figure 5.11 and 5.12).

The decrease in aortic diameter was correlated with an almost simultaneous decrease in pressure. The systolic pressure decreased to 100 mm Hg from 135 mm Hg and the diastolic pressure decreased to 75 mm Hg. Also, during this part of the protocol, a mean pressure of 83 mm Hg was recorded.

This decrease in pressure was expected because of the hemorrhage. It is worth noting that although the pressure decreased fairly rapidly, after approximately 3 minutes the pressure waveforms were steadily increasing towards normal values. Physiologically, the decrease in pressure decreases the rate of discharge in the aortic baroreceptors. Consequently, vasoconstriction takes place in the periphery and sympathetic input to the heart is increased in an effort to restore blood pressure (Ganong, 1993). The heart rate

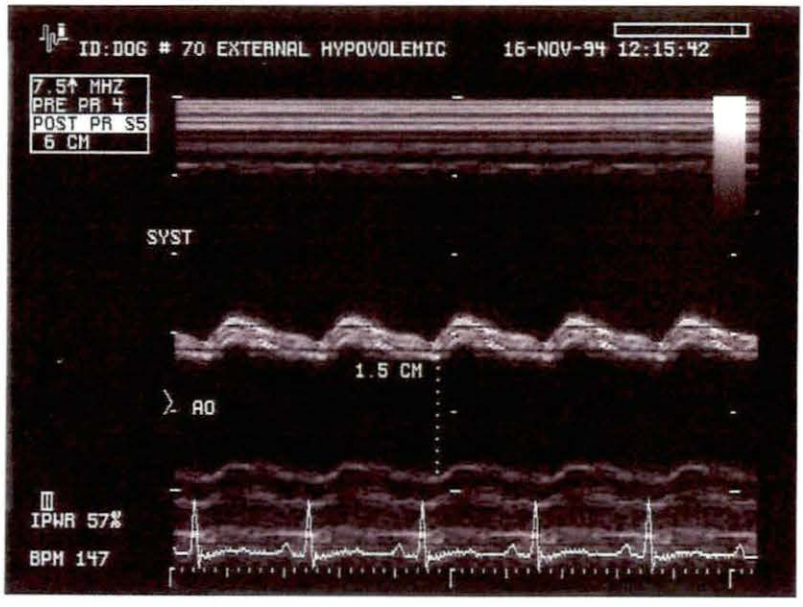

Figure 5.9: M-mode image during systole following the first hemorrhage period (Dog #4, prior to thoracotomy).

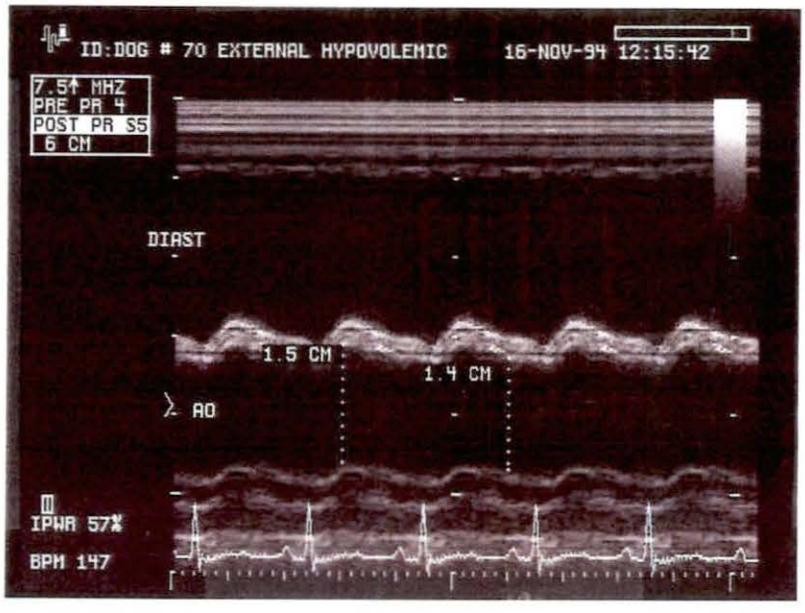

Figure 5.10: M-mode image during diastole following the first hemorrhage period (Dog #4, prior to thoracotomy).

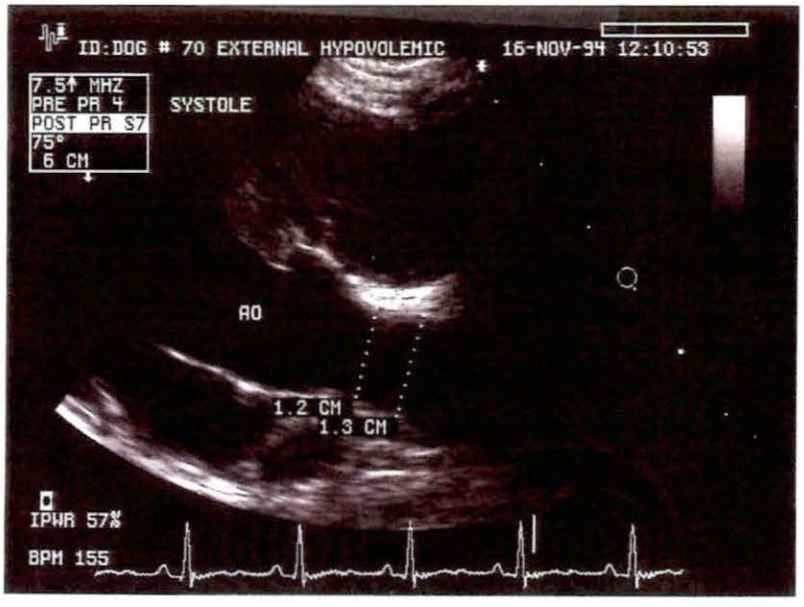

Figure 5.11: Two-dimensional image during systole following the first hemorrhage period (Dog #4, prior to thoracotomy).

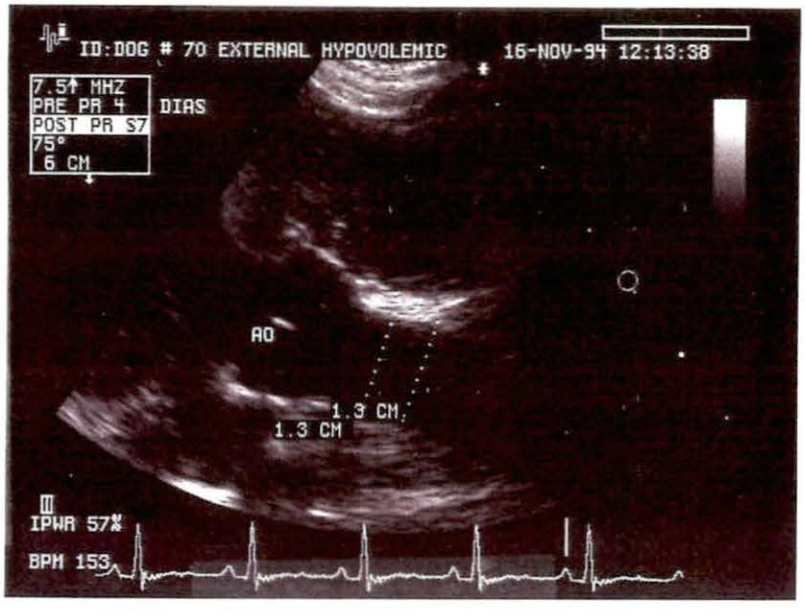

Figure 5.12: Two-dimensional image during diastole following the first hemorrhage period (Dog #4, prior to thoracotomy).

also increased due to the sympathetic system. The ascending aorta is becoming less distended because of the decrease in blood volume and thus, a decrease in aortic diameter is observed.

Having taken the diameter measurements needed during the first hemorrhage period, the next procedure in the experiment was to perform a second hemorrhage in order to reduce the total blood volume by thirty percent. This was done approximately fifteen minutes after the first removal of blood. After removing 30% of the total blood volume of dogs #4 and #5, the diameter decrease was clearly marked in the ultrasound images.

Table 5.3 outlines the mean results of dogs #4 and #5 after the second hemorrhage period. As expected, M-mode diastolic images showed a sharp decrease in diastolic aortic diameter from 1.7 cm (control value prior to hemorrhage and thoracotomy) to 1.3 cm (see Figures 5.13 and 5.14). This represents a 23.5% diastolic aortic diameter decrease. Moreover, the 2-dimensional images also showed a decrease from 1.5 cm to 1.2 cm which is equivalent to a 20% aortic diastolic diameter decrease from the control value (see Figures 5.15 and 5.16).

The systolic diameter values also decreased. The systolic diameter measured from the M-mode decreased from 1.5 cm, to 1.3 cm after the blood volume was reduced by thirty percent. This represents a 13.3% decrease from the control values. In addition, the systolic diameter measured from the 2-dimensional scan was reduced by 26.7% from 1.5 cm to 1.1 cm.

The pressure also decreased drastically from a systolic pressure of 100 mm Hg at the end of the first hemorrhage period to a systolic pressure of 60 mm Hg at the end of the second hemorrhage period. The diastolic pressure decreased from 75 mm Hg to 40 mm Hg. The mean pressure recorded following the second hemorrhage was 46 mm Hg.

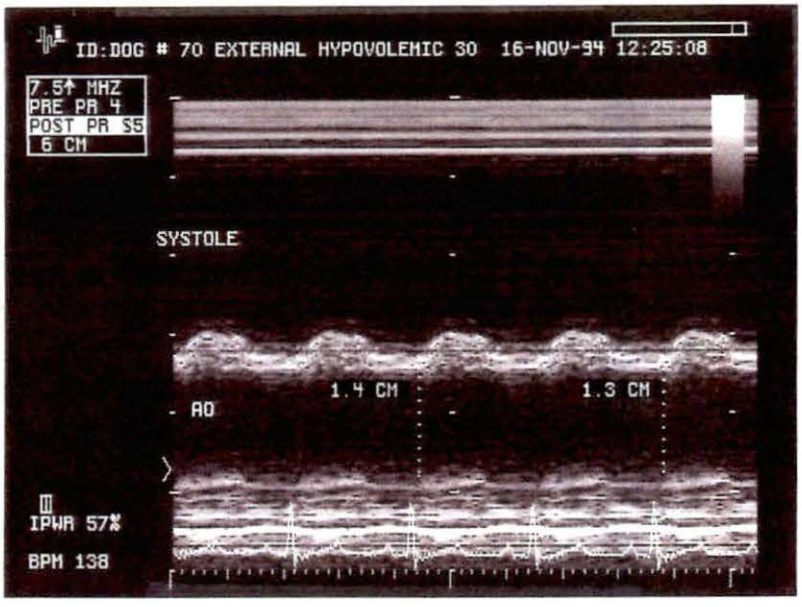

Figure 5.13: M-mode image during systole following the second hemorrhage period (Dog #4, prior to thoracotomy).

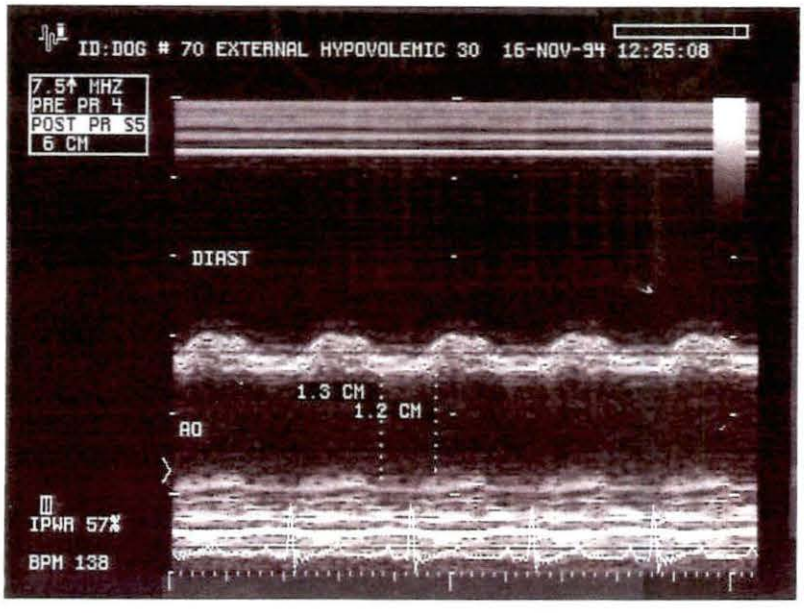

Figure 5.14: M-mode image during diastole following the second hemorrhage period (Dog #4, prior to thoracotomy).

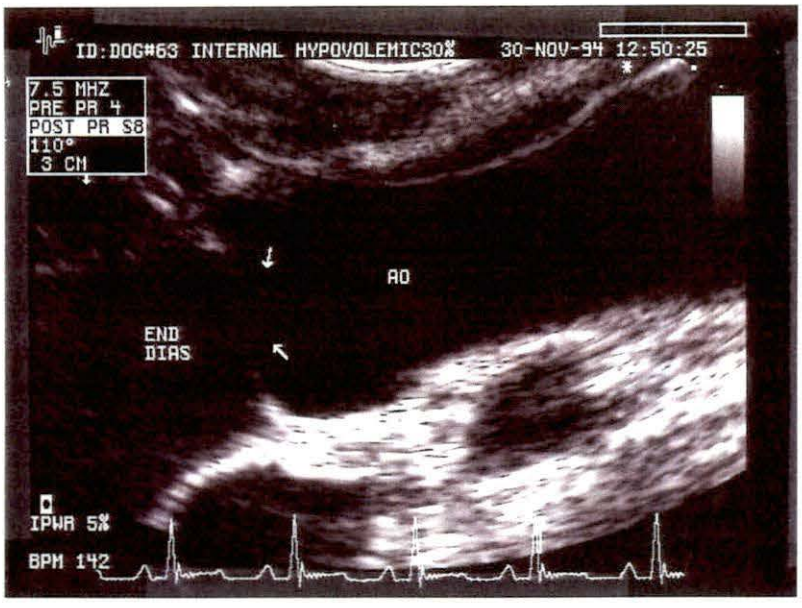

Figure 5.15: Two-dimensional image taken following the second hemorrhage period and prior to thoracotomy. The arrows are pointing in the direction of the aortic valve (Dog #5).

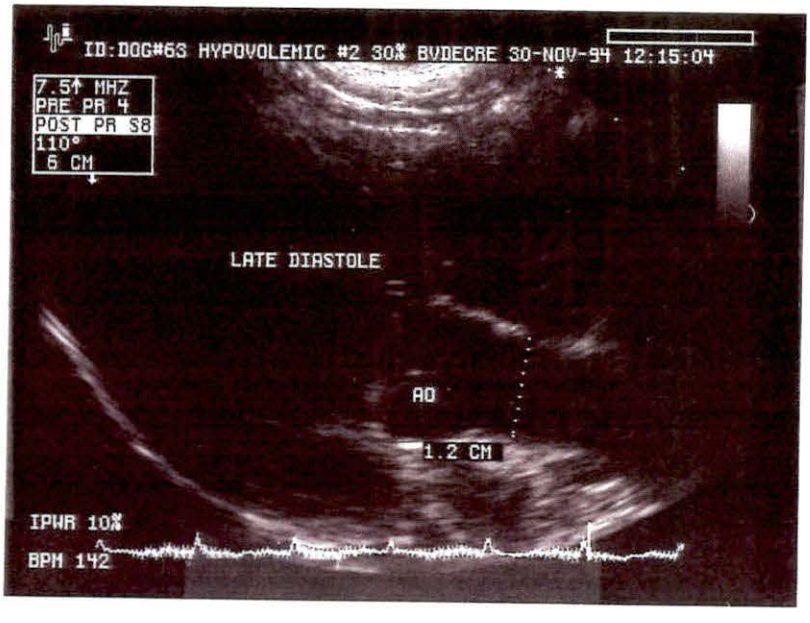

Figure 5.16: Two-dimensional image during late diastole following the second hemorrhage period (Dog #4, prior to thoracotomy).

The final phase in this experiment was to perform a thoracotomy through the sternum and record the aortic diameter invasively. For this part of the protocol, the ultrasonic probe of the workstation was placed on the aorta. Since the transducer needed to be acoustically coupled to the aorta, a spacer filled with conductive gel was placed between the transducer and the vessel. Table 5.3 summarizes the final results of dog #4 and #5.

During a small fraction of the surgery, dog #5 suffered from hypoxia. The pressure was elevated, the respiration rate and heart rate were very high. No measurements were taken during this phase of the experiment (see Figure 5.17 and 5.18). In these images the t-wave of the electrocardiogram is very large. This is usual in hypoxic cases. Once the respiration rate and heart rate were within normal ranges, measurements were taken. The mean pressure during this procedure was 56 mm Hg.

The aortic diameter after the two hemorrhagic periods approached the mechanical measurement value of 1.16 cm recorded following euthanasia. Diastolic diameter values of 1.2 cm using the M-mode (see Figures 5.19 and 5.20) and 1.2 cm using the 2-dimensional scan (see Figures 5.21 and 5.22) were calculated by the ultrasound workstation. These values represent a very small difference from the mechanical measured value. M-mode images and 2-dimensional images gave a 3.4% difference from the expected measured value. Likewise, systolic diameter values in this part of the experiment approached the mechanical value. M-mode images produced a 5.2% difference and 2-dimensional images gave a 3.4% deviation form the mechanical measured value.

This experiment confirmed the initial hypothesis that the ascending aortic diameter will decrease and approach the mechanical value as the blood volume is reduced. This decrease in aortic diameter is due to the less distention of the aorta's

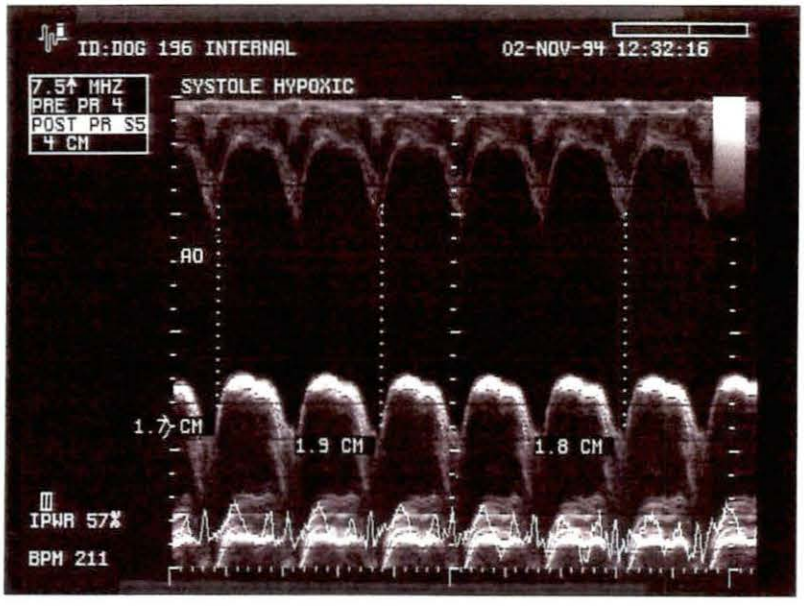

Figure 5.17: M-mode image illustrating hypoxia in experiment #2. The subject's heart rate increased and the t-wave in the electrocardiogram is very large (Dog #5).

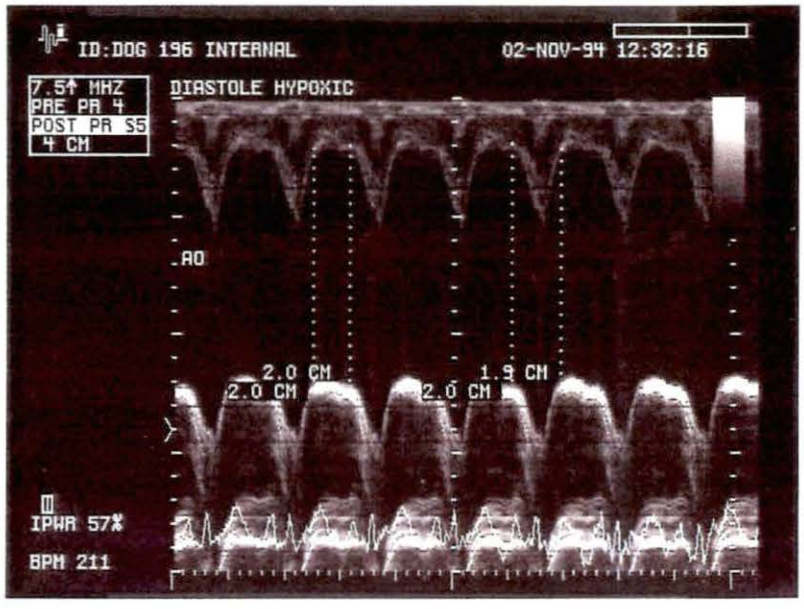

Figure 5.18: M-mode image illustrating hypoxia in experiment #2.

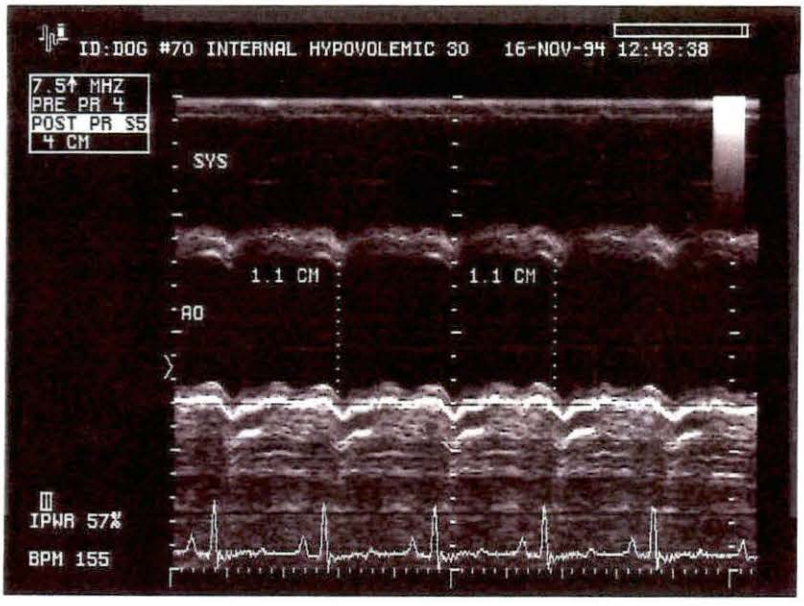

Figure 5.19: M-mode image taken following thoracotomy and after the second hemorrhage period. The transducer was placed directly on the ascending aorta (Dog #4).

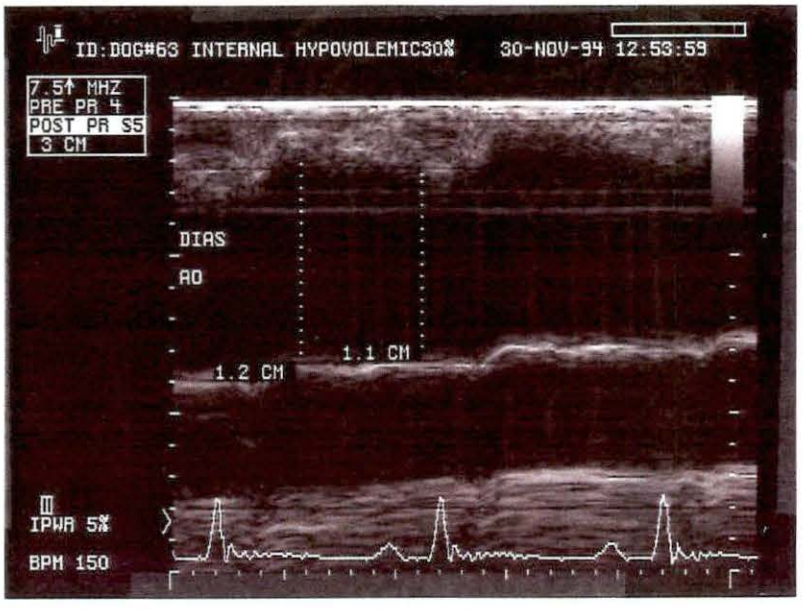

Figure 5.20: M-mode image taken following thoracotomy and after the second hemorrhage period. This scan was taken using the zoom function of the ultrasound workstation (Dog #5).

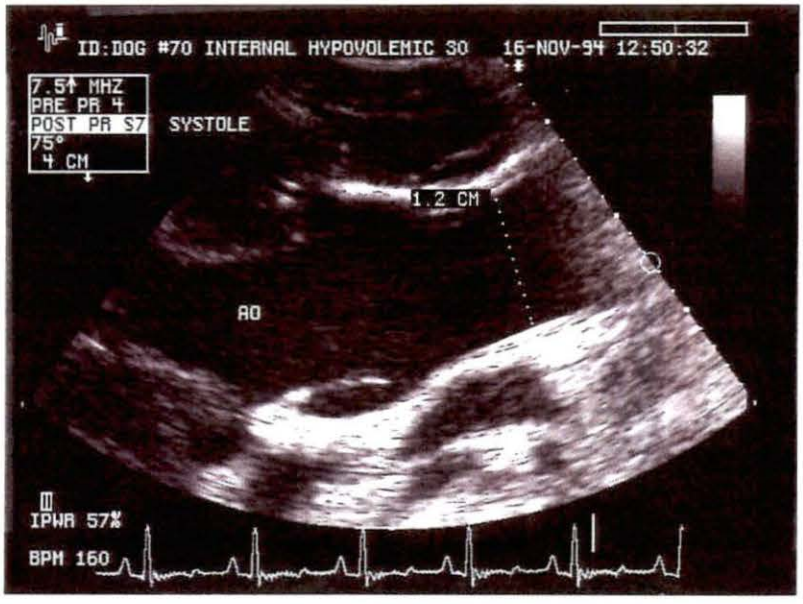

Figure 5.21: Two-dimensional scan during systole (Dog #4, following thoracotomy).

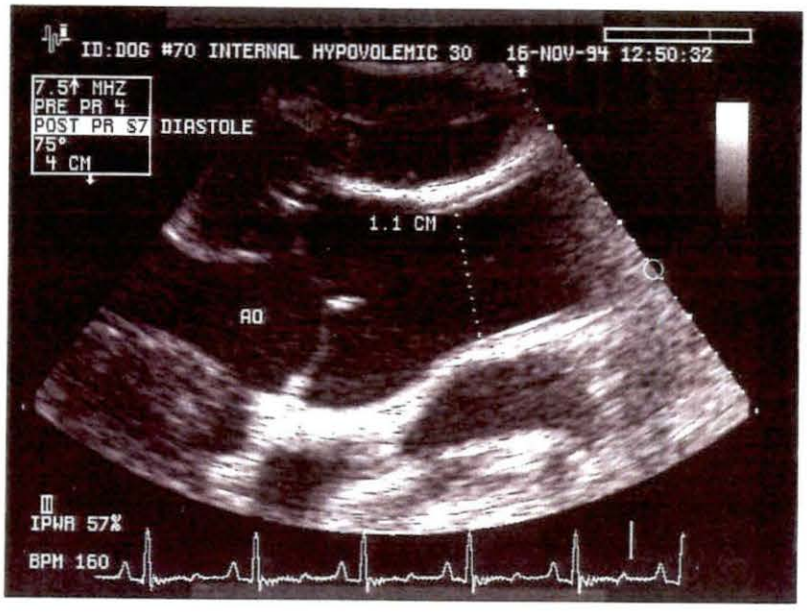

Figure 5.22: Two-dimensional scan during diastole (Dog #4, following thoracotomy).

elastic fibers, and not to the constriction of the aorta's vascular smooth muscle (Guyton 1986). The contraction of the muscular fibers can be neglected since they form a very small part of the aorta's composition.

Experiment 3: Hemorrhage induced after thoracotomy

For this experiment two dogs were studied. Refer to appendices G and H for the data tables and ultrasound images.

During the first part of the experiment, control readings of aortic diameter prior to the hemorrhage were made. The subjects were sedated using XBG sedative and placed in left lateral recumbency for the use of the ultrasound workstation. Table 5.4 summarizes the results for this part of the experiment.

The mean control values for the diastolic phase were 1.8 cm using M-mode analysis (see Figure 5.23 and 5.24) and 1.9 cm using the 2-dimensional scan (see Figure 5.25 and 5.26). Furthermore, the mean systolic diameter values given by the M-mode and the 2-dimensional views were 1.7 cm and 1.8 cm, respectively. These values are within the normal values of the canine ascending aorta for dogs weighing 15-20 Kg. The mean value for this range is 1.8 cm (Nelson and Couto, 1986).

During this procedure the maximum recorded systolic pressure was 120 mm Hg and the diastolic pressure was 80 mm Hg. A mean pressure of 93 mm Hg was recorded throughout the first stage of the experiment.

After the control recordings were taken, the animals were anesthetized with sodium pentobarbital (15 mg/kg). Following the thoracotomy, control measurements of the ascending aortic diameter were taken with the transducer probe along with the spacer placed directly on the artery. Table 5.4 outlines the results of the systolic and diastolic aortic diameter measurements taken using the ultrasound workstation.

Table 5.4: Aortic diameter mean values for experiment #3 (Dogs #6, #7)

Type of Measurement	M-mode view (cm)	2-dimensional view (cm)	Pressure (mm Hg)	Mechanical measurement (cm)	Heart Rate (BPM)
A. Control values prior to hemorrhage and thoracotomy					
Systole	1.7	1.8	Mean = 93	1.32 (± 0.026)	113
Diastole	1.8	1.9	120/80		
B. Control values following thoracotomy					
Systole	1.7	1.6	Mean = 100	1.32 (± 0.026)	130
Diastole	1.9	1.8	140/80		
C. Values following 15% total blood volume decrease					
Systole	1.4	1.2	Mean = 63	1.32 (± 0.026)	140
Diastole	1.5	1.3	80/55		
D. Values following 30% total blood volume decrease					
Systole	1.2	1.2	Mean = 48	1.32 (± 0.026)	135
Diastole	1.3	1.2	75/35		

Note: (± SD)

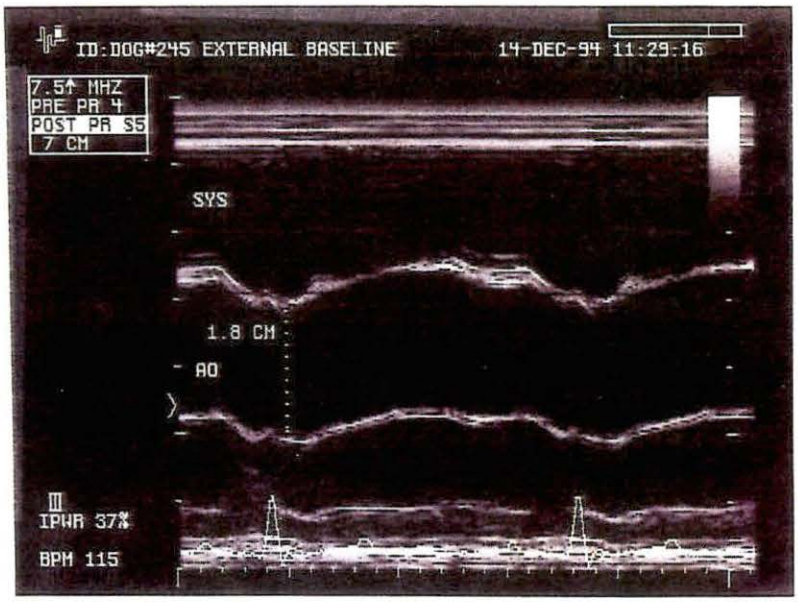

Figure 5.23: M-mode scan taken during the control values for experiment #3 (Dog #7).

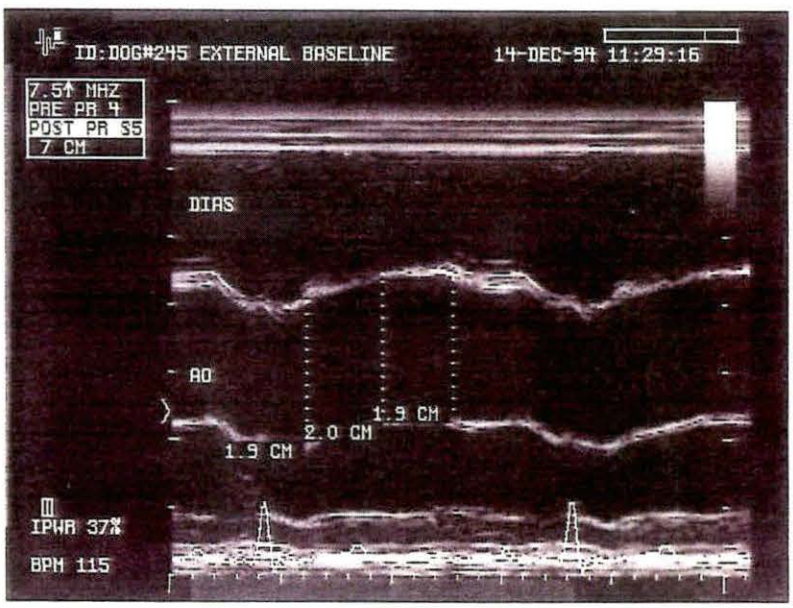

Figure 5.24: M-mode image illustrating the measurements of the ascending aortic diameter during diastole. This scan was taken during the external control period (Dog #7).

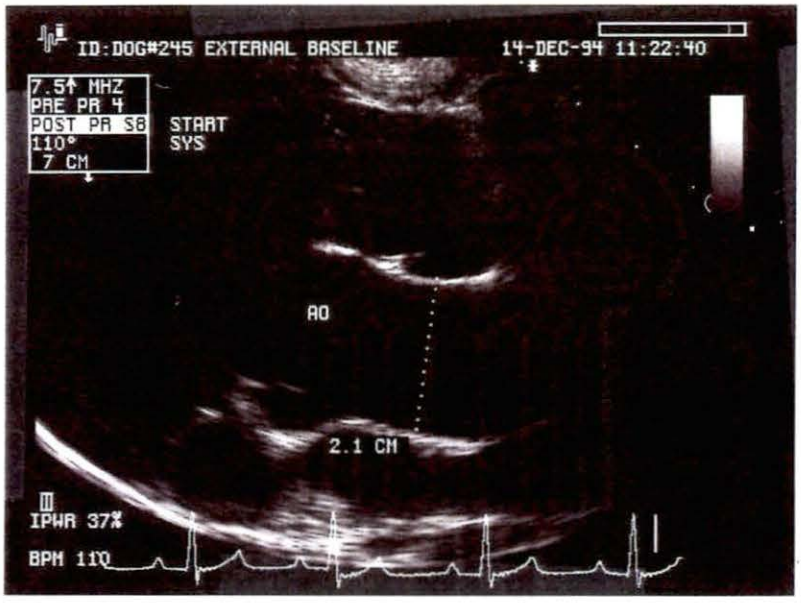

Figure 5.25: Two-dimensional image showing the diameter of the ascending aorta at the beginning of systole (Dog #7).

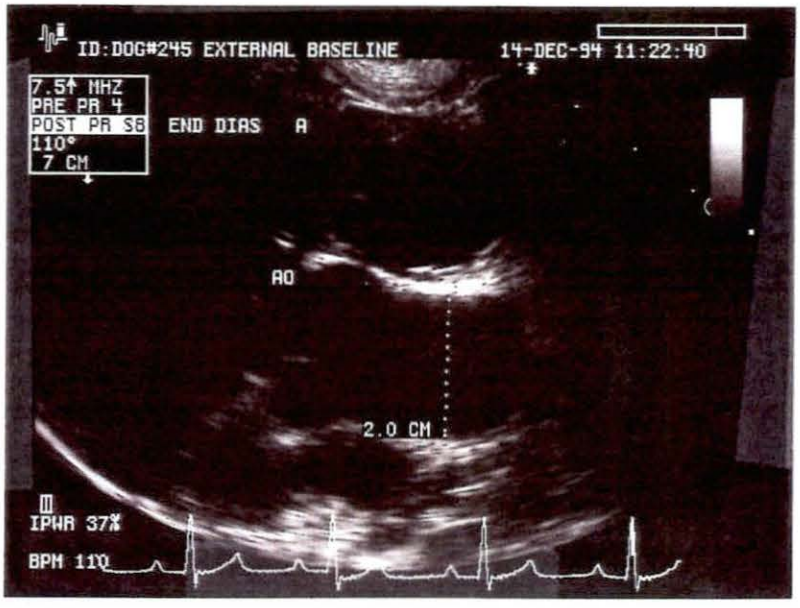

Figure 5.26: Illustration of the diameter of the ascending aorta at the end of diastole (Dog #7).

As can be seen in Table 5.4, the M-mode recordings following thoracotomy were close to the control values prior to thoracotomy. The systolic diameter read 1.7 cm, the same as the external control value. In addition, the diastolic diameter recorded was 1.9 cm which differed from the control value prior to thoracotomy by only 5.3% (see Figures 5.27 and 5.28).

Likewise, the measurements from the 2-dimensional scan recordings were very close to those prior to thoracotomy. The systolic diameter measured was 1.6 cm, and the diastolic diameter was 1.8 cm. These values represent approximately 5.3% difference and 6% difference in systolic and diastolic diameters respectively (see Figures 5.29 and 5.30). While the control values following thoracotomy were being taken, the mean pressure recorded by the transducer was 100 mm Hg. Systolic pressure increased slightly to 140 mm Hg, whereas the diastolic pressure stayed constant at 80 mm Hg.

Following these control measurements, the large cannula was inserted into the animal's femoral artery for the hemorrhage. Again, fifteen percent of the total blood volume was removed. For dog #6, weighing 18.6 kg, the estimated total blood volume was 1.77 liters; therefore, 265 ml were removed. Dog #7 weighed 15 kg at the time of surgery. The estimated total blood volume was 1.43 liters and 214 ml were removed during the first hemorrhagic period.

Drastic diameter and pressure decreases were observed after the removal of the first 15% of blood in both dogs. The M-mode view showed a decrease in diameter from 1.7 cm to 1.4 cm in systole. This represents a 17.6% in diameter decrease in the systolic phase. Also, diastolic diameter decreased sharply, from 1.9 cm in the control values to 1.5 cm after the first hemorrhagic period. The diameter value was reduced approximately 21% in the diastolic phase (see Figure 5.31 and 5.32). During this period the mean pressure decreased to 63 mm Hg.

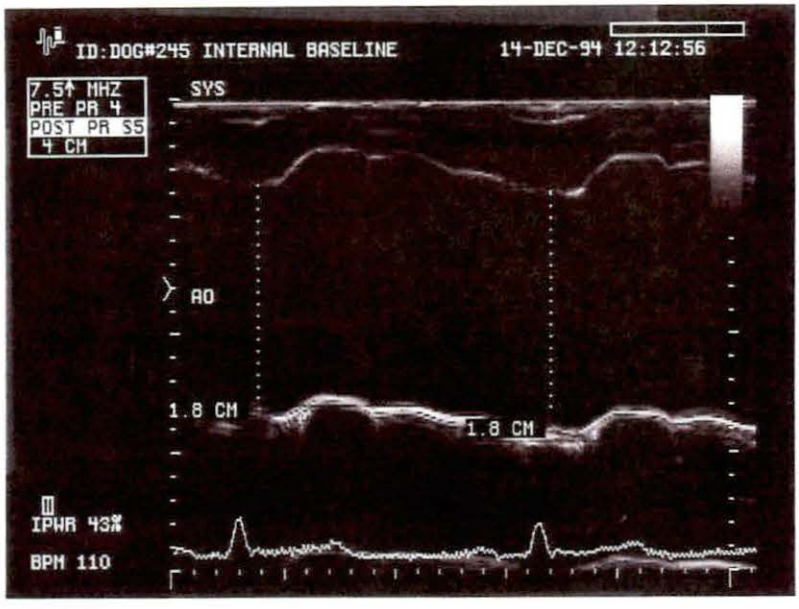

Figure 5.27: M-mode image during systole and prior to hemorrhage (Dog #7, following thoracotomy).

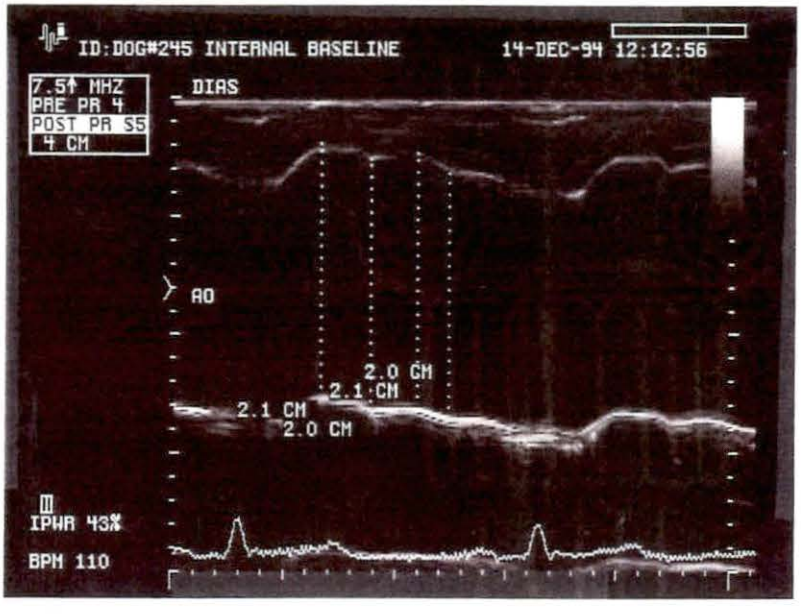

Figure 5.28: M-mode image during diastole prior hemorrhage (Dog #7, following thoracotomy).

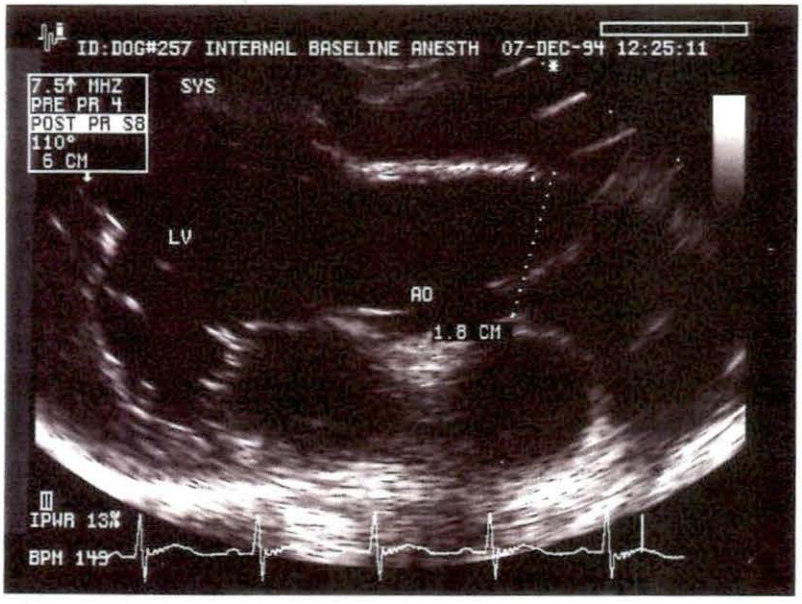

Figure 5.29: Two-dimensional image taken during the internal control recordings. The left ventricle and the aortic root are shown in the image (Dog #6).

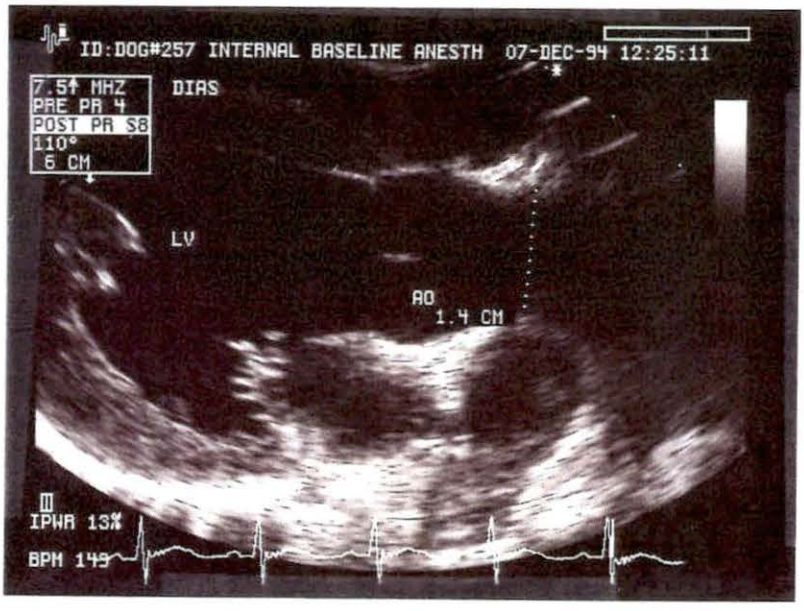

Figure 5.30: Two-dimensional image illustrating the diastolic phase during the internal control recordings (Dog #6).

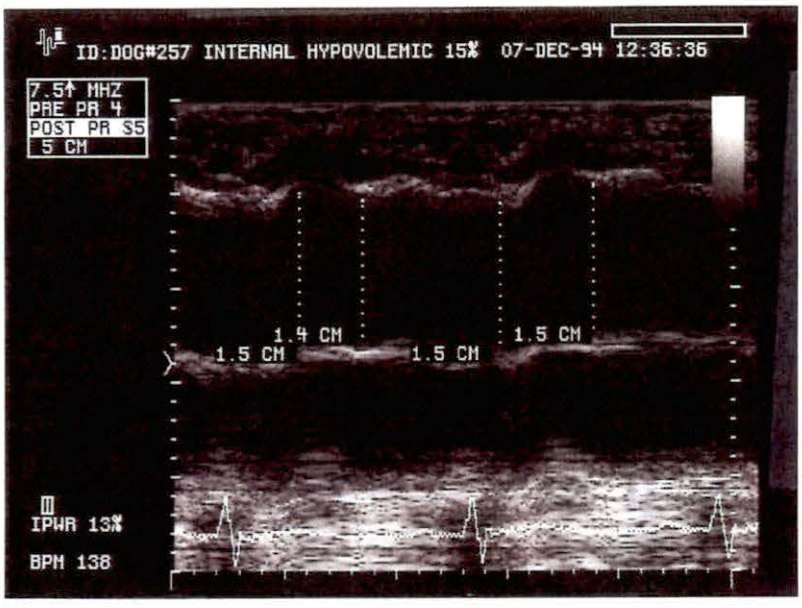

Figure 5.31: M-mode image during systole after the first hemorrhage period (Dog #6).

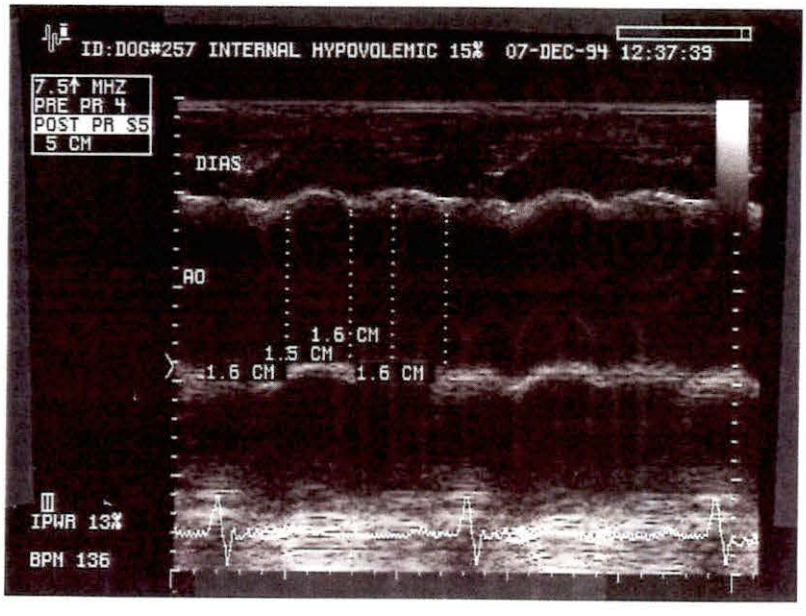

Figure 5.32: M-mode image during diastole after the first hemorrhage period (Dog #6).

For comparison purposes the 2-dimensional images were analyzed. It has been shown that M-mode images and two dimensional images follow the same pattern. The systolic diameter decreased from 1.6 cm in the invasive control to 1.2 cm after the first bleeding. This represents a 25% decrease in aortic diameter during the systolic phase. The diastolic diameter was 1.3 cm. It was reduced approximately 27.8% from its original value of 1.8 cm recorded in the control value (see Figures 5.33 and 5.34). The mean mechanical measurement of the ascending aortic diameter for this experiment was 1.32 cm.

The second hemorrhagic period began approximately fifteen minutes after the first. Both the M-mode and the 2-dimensional images registered a further decrease in aortic diameter. Using the M-mode, systolic diameter decreased to 1.2 cm and the diastolic diameter was reduced to 1.3 cm. The overall per cent decrease (from the control values following thoracotomy as reference) was 29.4% for systole and 31.6% for diastole. In addition, these values were close to the mean mechanical value of 1.32 cm. Systolic diameter had a 9.1% difference for the mechanical measurement and the diastolic diameter only differed by 1.5% (see Figures 5.35 and 5.36). The 2-dimensional images also showed a marked decrease in diameters. The systolic aortic diameter was 1.2 cm, a 25% reduction from the control value. The diastolic diameter decreased to 1.2 cm from 1.8 cm. This represents a 33.3% diameter reduction (see Figure 5.37 and 5.38). At this point of the experiment the mean pressure recorded was 48 mm Hg. The systolic pressure was 75 mm Hg and the diastolic pressure was 35 mm Hg.

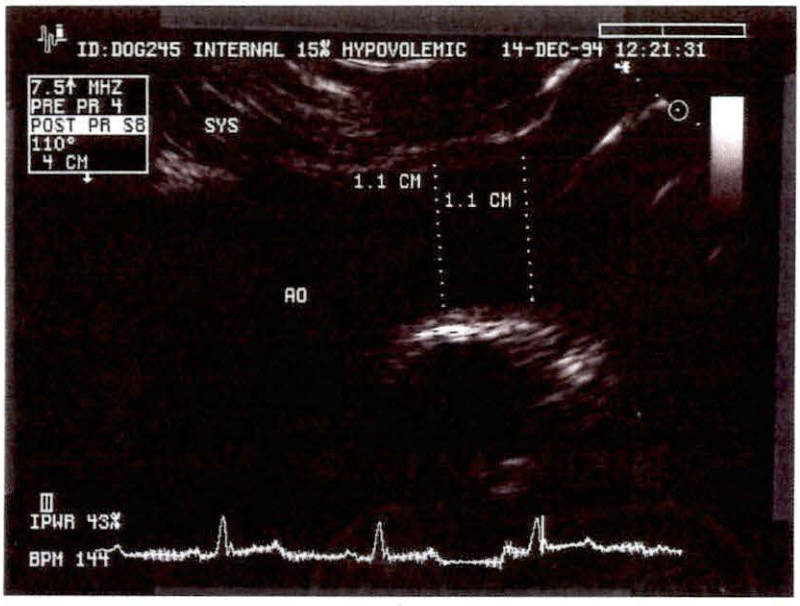

Figure 5.33: Two-dimensional image during systole after the first hemorrhage period (Dog #7, following thoracotomy).

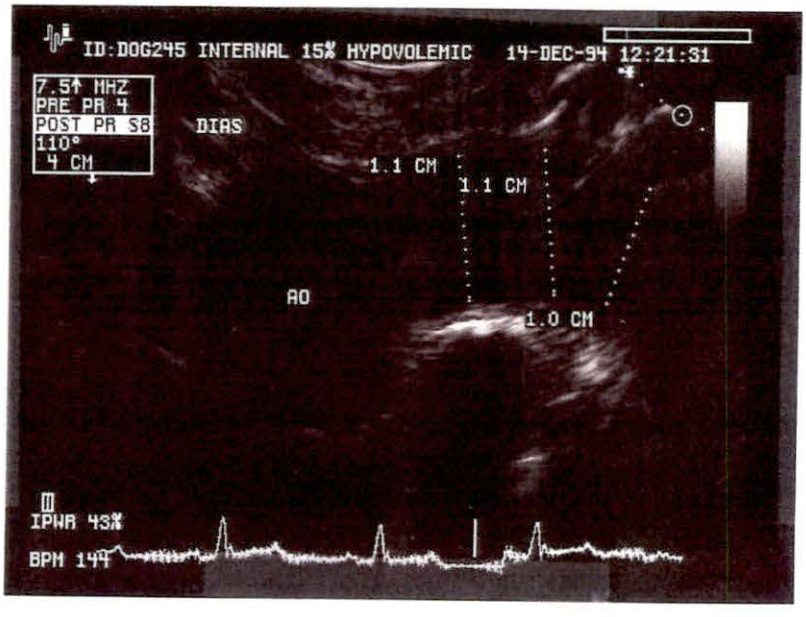

Figure 5.34: Two-dimensional image during diastole after the first hemorrhage period (Dog #7, following thoracotomy).

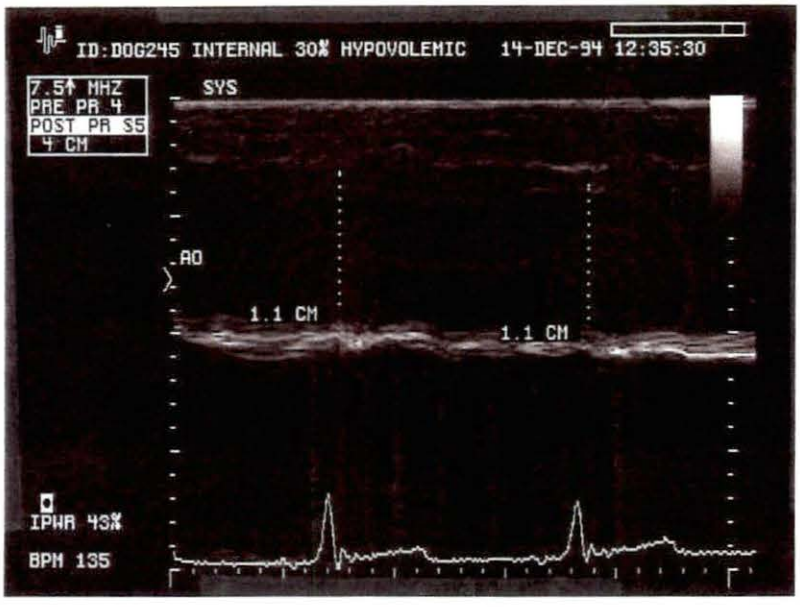

Figure 5.35: M-mode image during systole illustrating the ascending aortic diameter decrease following the second hemorrhage period (Dog #7).

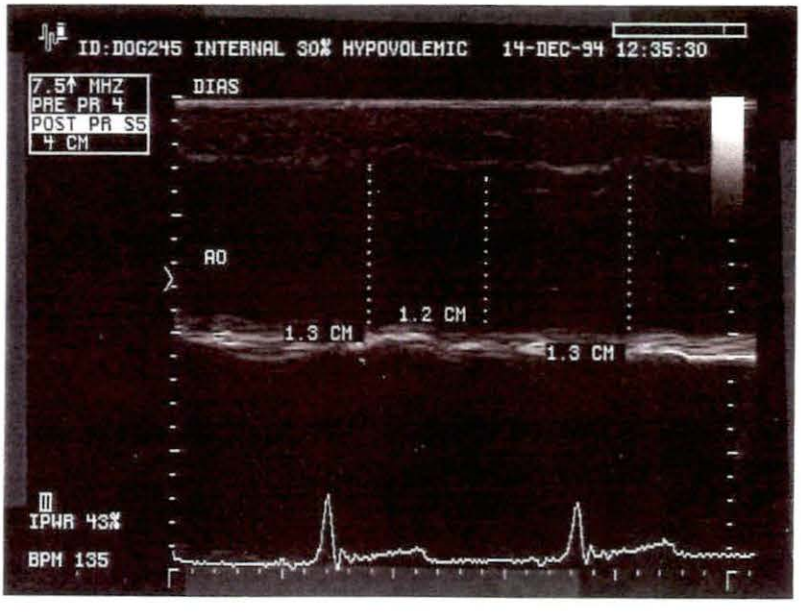

Figure 5.36: M-mode image during diastole illustrating the ascending aortic diameter decrease following the second hemorrhage period (Dog #7).

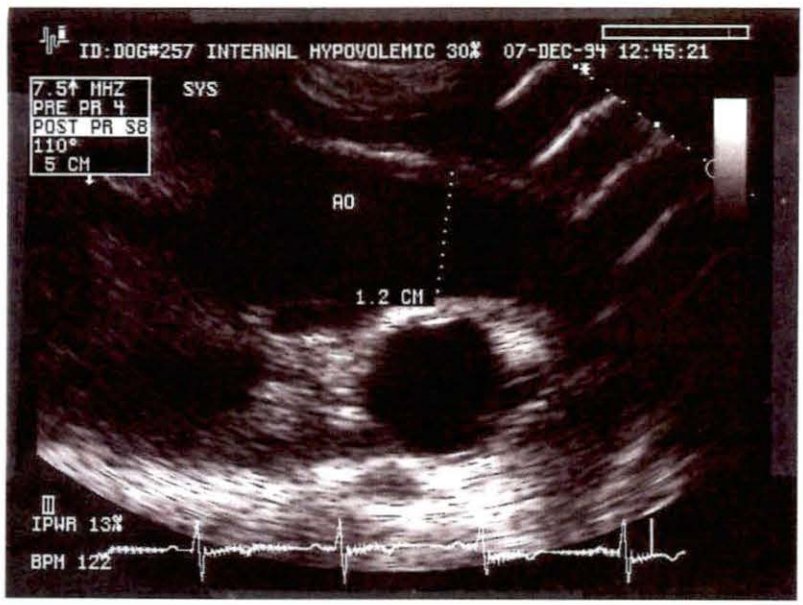

Figure 5.37: Two-dimensional scan during systole after the second hemorrhage period (Dog #6).

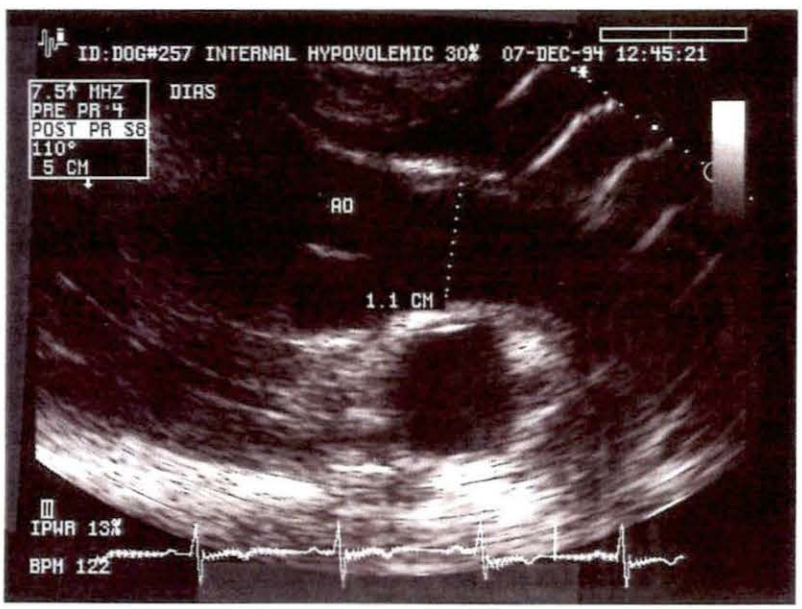

Figure 5.38: Two-dimensional scan during diastole after the second hemorrhage period (Dog #6).

CHAPTER 6: DISCUSSION

In this chapter the data collected from the experiments were analyzed to study the relationship between the weight of the subjects and their corresponding ascending aortic diameter.

Relationship between diameter and weight

The canine ascending aortic diameter can be estimated by running a linear regression to the data shown in Table 6.1.

The correlation coefficient (r) for the systolic diameter is 0.82 and that for diastolic measurements is 0.84. This indicates a high correlation between the weights of the subjects and the diameters of their ascending aorta.

Table 6.1: Weight and diameter correlation: Non-invasive mean values

Dog number	Weight (kg)	Systolic diameter (cm)	Diastolic diameter (cm)
1	22.2	2.0	2.2
2	18.6	2.0	2.0
3	12.2	1.7	1.8
4	12.2	1.7	1.8
5	12.2	1.4	1.6
6	18.6	1.8	1.8
7	15.0	1.7	1.9

Figures 6.1 and 6.2 show a graphical representation of the systolic and diastolic phases diameter, together with the best fit line through these points. By knowing the weight of the dog, the diameter of the ascending aorta could be interpolated in these graphs. From these figures one can easily determine that as the weight of the dog increases, the diameter of the ascending aorta will steadily increase in a linear fashion.

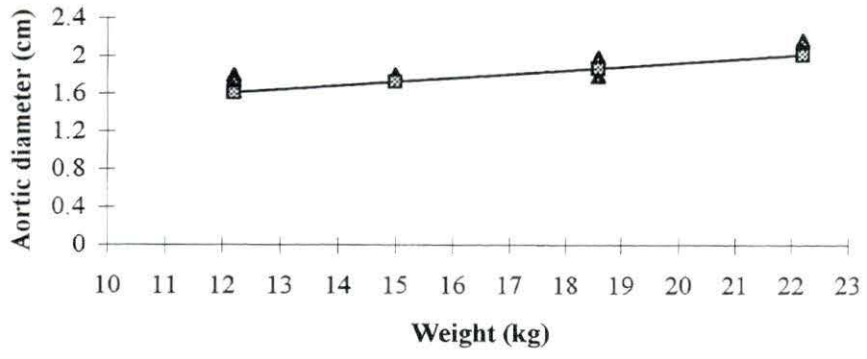

Figure 6.1: Diameter-weight relationships (diastole).

A commonly used statistical rule in interpreting whether two variables are related to each other is by analyzing the correlation coefficient value (r). Statistically, if there is less than one chance in twenty ($P = 0.05$) that the value will occur, then the r value is regarded as significant.

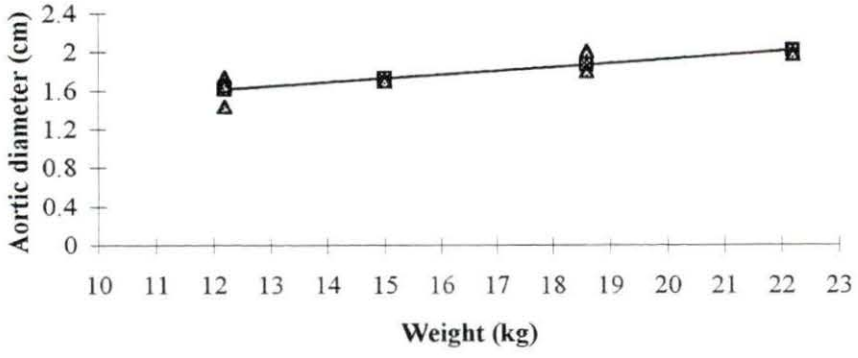

Figure 6.2: Diameter-weight relationships (systole).

Since the data shown in Table 6.1 gave a value for the correlation coefficient (r) equal to 0.82 and 0.84 for systole and diastole respectively, one can be reasonably sure that this indicates a true correlation not a random occurrence.

From Figures 6.1 and 6.2 the systolic and diastolic ascending aortic diameter values can be compared. In this experiment the diastolic diameter values are slightly higher than the systolic diameter values. This can be seen if both graphs are superimposed. However, physiologically, the systolic diameter must be higher than their diastolic counterparts. During systole, the heart muscle is contracting and forcing blood out from the left ventricles to the ascending aorta. Since the equipment used in this experiment did not allow us to measure accurate diameter changes, the behavior of the curve must be studied instead of the numerical values recorded for both systole and

diastole. Also, the slope of the best fit line of both systolic and diastolic diameters is parallel, which means that they have the same slope.

CHAPTER 7: CONCLUSIONS

Error sources

Placement of the ultrasound transducer is critical in obtaining scans useful in Doppler diameter analysis, and success proved to be a difficult task with some of the subjects used. With the deep chested dogs studied, difficulties arose in placing the transducer in a position allowing echoes to be taken directly along the axis of the heart and aortic root; a variable scan depth sometimes was not sufficiently deep to provide scans below the rib cage where the correct scan angle is more easily obtained. With humans the required apical long axis view of the heart is commonly obtained by placing the transducer in the supra-sternal position. Accurate aortic diameter and flow velocities are frequently acquired for use in clinical cases from this orientation.

Lack of precision in diameter measurements using the Interspec ultrasound workstation is possible since the diameter measurements were taken in centimeters with only one decimal place. Unfortunately, the level of sensitivity of the machine was not sufficient to make accurate diameter measurements corresponding to systole and diastole.

This error factor could be reduced by upgrading the software installed in the equipment. By doing so, the diameter changes could be recorded with up to three significant figures, and certainly the systolic diameter measurements would be higher than the diastolic diameter values. Also, improvements could be made by incorporating a zoom function into the system. This function allows for image magnification while the screen resolution remains constant. Moreover, error potential can be minimized by reducing the original scan depth, or by increasing monitor size without changing screen snap. The snap is the smallest measurable distance of the system. All three modifications would result in a calibration in which the screen resolution represents a smaller actual distance.

Another potential error introduced into this research is the assumption that the venous return is decreasing while the subject is undergoing hemorrhage. Sometimes blood pressure recordings can be misleading when hemorrhage is induced. Theoretically, as the heart is losing blood through hemorrhage, the stroke volume will decrease because of decreased venous return. However, this can only be assumed in this project. The only way one can know for sure that the venous return has decreased is by calculating the gradient flow venous return. This gradient is calculated by taken the systemic filling pressure, $\mathbf{P_{sf}}$, which is usually 7 mm Hg, and subtracting this value from the right atrial pressure. In a normal heart, the right atrial pressure should be near zero so that the gradient will be close to 7 mm Hg. With this gradient, the blood will be pushed back to the heart and venous return will be maintained. In a failing heart, the right atrial pressure

will increase and, therefore, the gradient will decrease. Consequently, the venous return will decrease.

Future potential for studies

In order to calculate the aortic compliance, or elasticity, non-invasively, the next step in this study would be to correlate pressure measurements taken by the transducer with values obtained by a non-invasive method to calculate pressure. A possible technique would be by studying the flow velocity in the aorta of the dogs. Application of the following formula might be of use when making pressure measurements non-invasively (from Bernstein, 1978):

$$\mathbf{P} = 4 \times (\mathbf{V})^2 \qquad (7.1)$$

where **P** is the pressure expressed in millimeters of mercury, and **V** is the flow velocity term, in meters per second, squared. However, equation 7.1 gives the value of the pressure drop across a valve. Depending upon where in the flow stream the velocity is measured, the values for pressure may not be truly representative of actual maximum values. This would be the case in both laminar and turbulent flow profiles, since both exhibit variations in flow velocity across the flow stream. Data needs to be obtained before confident judgments about the validity of Doppler measurements in pressure can be made. Moreover, investigation into the application of this formula to the canine aortic root needs to be conducted. This common clinical cardiology formula may have restricted application to the aortic root and/or to dogs.

Another factor that must be highlighted in this project is the pressure measurements. As mentioned in Chapter 4, the pressure recordings were made at the level of the femoral artery during the hemorrhage. This is not a true value for the pressure directly in the aortic root. Figure 7.1 shows the pressure changes in the arteries in the periphery of the body for a standing man. As can be seen, Figure 7.1 the systolic pressure is higher than the expected pressure in the aorta. As one moves away from the aorta, the systolic pressures of the arteries in the periphery will be significantly higher than the pressure encountered in the aortic arch. The diastolic pressure, however, stays fairly constant in different regions of the body. This concept can be applied to a dog in dorsal recumbency.

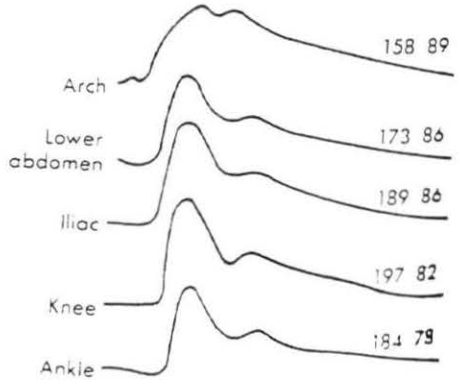

Figure 7.1: Relationship between pressure in the aorta and other arteries (Berne and Levy, 1990).

To make an accurate estimation of how much the aortic pressure is changing because of the hemorrhage, a high fidelity transducer tipped catheter must be passed through the carotid artery into the root of the aorta. Thus a canulation of the carotid artery would be implemented as a future change in the protocol

Aortic compliance estimation

The ultrasound workstation used in this research project (see Appendix A for specifications) proved to lack the sensitivity needed to distinguish between fine levels of systolic and diastolic diameter changes. Since this machine is mostly used in pediatric laboratories, the level of sensitivity for distance measurements is not very high. Consequently, the machine is not able to distinguish changes in the order of millimeters. The software used in the ultrasound workstation did not allow accurate calculation of diameters for systole and diastole. It rounded off the values to one significant digit.

If the equipment had allowed us to make accurate recordings of the ascending aortic diameter, an estimation of aortic compliance could be attempted as described in the following section.

Compliance calculations

Aortic compliance is defined by the Food Drug Administration as the change in volume divided by the corresponding change in blood pressure at the level of the aorta.

Based on the following equation (Ganong, 1993):

$$\mathbf{C} = \Delta\mathbf{V} / \Delta\mathbf{P} \tag{7.2}$$

where **C** is the compliance value, **V** is the volume in mm^3, and **P** is the pressure in mm Hg, a compliance value can be determined. Assuming the ascending aorta behaved as a cylinder, the volume could be calculated using the following volume equation:

$$\mathbf{V} = \Pi \times \mathbf{R}^2 \times \mathbf{H} \tag{7.3}$$

In this equation the radius (**R**) can be calculated from the diameter of the aorta taken by the ultrasound workstation and the height variable, or **H**, can be assumed to be 1 mm. In order to get the delta value (Δ), the systolic and diastolic volumes would be subtracted as outlined in Equation 7.4:

$$\Delta\mathbf{V} = \mathbf{V}_{(sys)} - \mathbf{V}_{(dias)} \tag{7.4}$$

For the pressure variable in Equation 7.2, the systolic and diastolic pressures, recorded by the pressure transducer during the experiments, would be subtracted as in Equation 7.5. This value is the equivalent of the pulse pressure of the subject:

$$\Delta\mathbf{P} = \mathbf{P}_{(sys)} - \mathbf{P}_{(dias)} \tag{7.5}$$

As the blood volume decreases in the cardiovascular system because of the hemorrhage, the muscular arteries in the periphery of the body are undergoing vasoconstriction. As the diameter of the vessels is decreasing, the flow in an artery will

increase and sometimes turbulent flow is encountered. The lack of blood in the cardiovascular system (due to hemorrhage) will decrease the compliance in the artery. In other words, the vessel will become stiffer.

Another factor to consider when making these aortic compliance calculations is the timing of the measurements following hemorrhage. If possible recordings of systolic and diastolic diameters must be made within one cardiac cycle. In this project measurements for the diameter and pressure were taken after the subject's cardiovascular system started to compensate for the loss of blood. For this reason, one cannot assume a decrease in venous return.

This increase in volume is directly related to the compliance calculations. As can be seen in the pressure-volume relationship (see Figure 7.2), the compliance represents the slope of this line. An increase in volume and a decrease in pressure will result in an increase in compliance, which in turn represents a less stiff vessel. On the other hand, a decrease in compliance (stiffer vessel) will be experienced with a decrease in volume and increase in blood pressure.

Finally, a decrease in compliance will be related to the vessel becoming stiffer, or less elastic. As this happens, there will be an increase in the total peripheral resistance at that region of the aorta. Consequently, the pulse pressure will increase and the ventricular ejection phase will be delayed and shortened. It will now take more time for the left ventricle to reach that higher peak systolic pressure. Since the volume of the

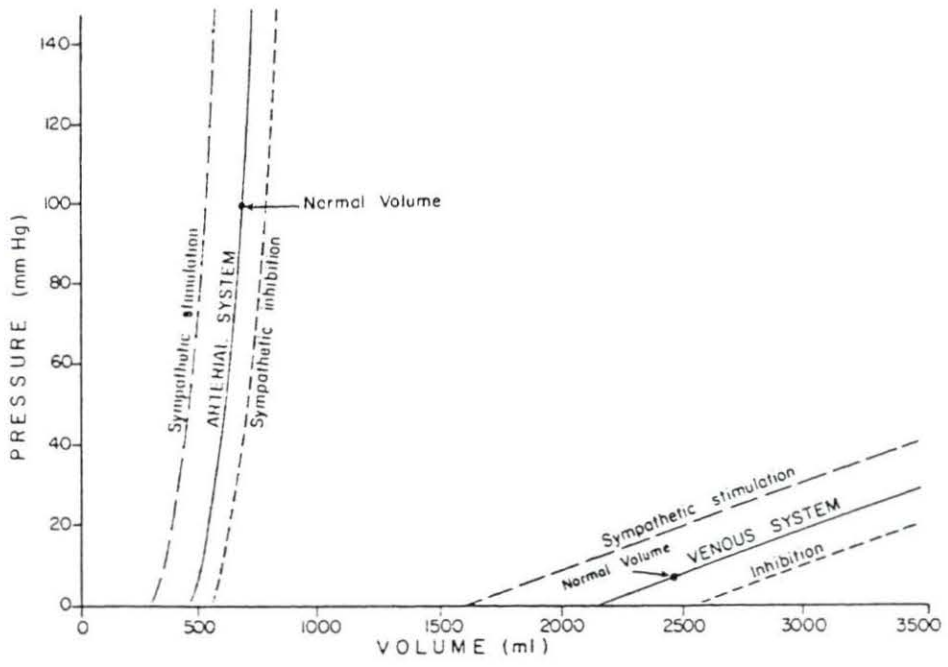

Figure 7.2: Pressure - volume relationships in the arterial and venous system (Guyton, 1986)

heart is smaller (length of the muscle fibers has decreased), there will be a decrease in stroke volume.

The method of estimation of arterial compliance presented in this section could be applied to the entire arterial system. However, further experiments and calculations must be made before an accurate prediction of compliance could be given at the level of the ascending aorta, specifically, during hemorrhage.

Final remarks

The preliminary aortic diameter study yielded unfavorable information about real potential for using an inexpensive, common ultrasound unit to obtain reliable aortic data. The diameter measurements taken supported that the pressure drops and diameter decreases were directly related to total blood volume reduction. However, as can be observed in Chapter 5, the diastolic diameter values recorded by the ultrasound workstation were slightly higher than the systolic diameter measurements.

To conclude, the ultrasound workstation used throughout this research proved to be unable to record ascending aortic diameter changes of the order of millimeters. Accurate measurements for the ascending aortic diameter values must be recorded in order to give an faithful estimation of aortic compliance. By increasing the sensitivity of the equipment, diameter measurements could probably be determined more accurately. This way systolic and diastolic values will certainly correspond to the expected values. Once this has been proven, this research project will have clinical significance for the medical field.

BIBLIOGRAPHY

Aars, H., 1971. Effects of Altered Smooth Muscle Tone on Aortic Diameter and Aortic Baroreceptor Activity in Anesthetized Rabbits. *Circulation Research.*; 28: 254-262.

Aars, H., 1969. Relationship Between Blood Pressure and Diameter of Ascending Aorta in Normal Hypertensive Rabbits. *Acta Physiologica Scandinava.*; 75:397- 405.

Archibald, J., 1965. Canine Surgery: A Text for Reference Work. American Veterinary Publications, Inc. California.

Barr, F., 1994. Diagnostic Ultrasound in the Dog and Cat. Library of Veterinary Practice. Blackwell Scientific Publications. Boston, Massachusetts.

Berne, R., Levy, M., 1990. Physiology. 3rd edition. Mosby Year Book. Boston, Massachusetts.

Bernstein, E., 1978. Noninvasive Diagnostic Techniques in Vascular Disease. The C.V. Mosby Co. St. Louis, Missouri.

Berrios, J., and Pedersen, P., 1994. Ultrasonic Measurement of Forced Diameter Variations in an Elastic Tube. *Ultrasonic Imaging.*; 16: 124-142.

Caro, C., Pedley, T., Schroter R., and Seed, W., 1978. The Mechanics of the Circulation. Oxford University Press. New York.

Cobbold, R., 1974. Transducers for Biomedical Measurements: Principles and Applications. John Wiley & Sons. New York.

Dennis, M., Nealeigh, R., Lee Pyle, R., Gilbert, S., Lee, A., and Miller, C., 1978. Echocardiographic Assessment of Normal and Abnormal Function in Beagle Dogs. *American Journal of Veterinary Research.*; 10: 1591-1598.

Dobrin, P.B., 1974. Physiology and Control of the Circulation. *Lex et Scientia..* 10(3):61-89.

Friedman, M., Roeske, W., Sahn, D., Larson, D., and Goldberg, S., 1982. Accuracy of M Mode Echocardiographic Measurements of the Left Ventricle. *The American Journal of Cardiology.*; 49: 716-723.

Friedwald, V., 1977. Textbook of Echocardiography. W.B. Saunders Company. Philadelphia, Pennsylvania.

Fleming, D., Ko, W., and Neuman, M., 1977. Indwelling and Implantable Pressure Transducers. CRC Press. Inc. Cleveland, Ohio.

Ganong, W.F. 1993. Review of Medical Physiology. 16 ed. Appleton and Lange. Norwalk, Connecticut.

Geddes, L. and Baker, L., 1989. Principles of Applied Biomedical Instrumentation. John Wiley & Sons Inc. New York.

Gordon, D., 1984. Ultrasound as a Diagnostic and Surgical Tool. The Williams and Wilkins Co. Baltimore.

Guyton, A. 1986. Textbook of Medical Physiology. 7 ed. W. B. Saunders Company. Philadelphia, Pennsylvania.

Hadjicostis, A. , and Hottinger, C. 1984. Ultrasonic Transducer Materials for Medical Applications. *Ferroelectrics.*; 60: 107-126.

Han, C., and Hurd, C, . 1994. Practical Guide to Diagnostic Imaging: Radiography and Ultrasonography. American Veterinary Publication. Goleta, California.

Hasson, J. E., Megerman, J., and Abbott, W. M. 1985. Increased Compliance Near Vascular Anastomoses. *Journal of Vascular Surgery.*; 21:163-170.

Heibig. J., 1983. A Primer of Echocardiography. John Wright & Sons, Great Britain.

Hoenig, S., and Scott, D., 1977. Medical Instrumentation and Electrical Safety. John Wiley & Sons Inc., New York.

Labs, K., Jager, K., Fitzgerald, D., Woodcock, J., and Neuerburg-Heusler, D., 1992. Diagnostic Vascular Ultrasound. Hodder & Stoughton. London.

Leonard, E., 1968. Fundamentals of Small Animal Surgery, W. B. Sanders Co. Philadelphia, Pennsylvania.

Lombard, C., 1983. Normal Values of the Canine M-mode Echocardiogram. *American Journal of Veterinary Research.*; 45: 2015- 2018.

Manax, W., Bloch, J., Longerbeam, J., and Lillehei, R., 1963. Plastic Adhesive as an Adjunct in Suture Anastomoses of Small Blood Vessels. *Surgery.*; 54: 663-667.

McDicken, W., 1976. Diagnostic Ultrasonics. John Wiley & Sons Inc., New York.

Meerbaum, S., Meltzer, R., 1989. Myocardial Contrast Two-Dimensional Echocardiography. Kluwer Academic Publisher. New York.

Miles, K., 1989. Basic Principles and Clinical Applications of Diagnostic Ultrasonography. *Compendium on Continuing Education for the Practicing Veterinarian.*; 11: 609-622.

Miller, Malcolm E. 1986. Anatomy of the Dog. W.B. Saunders Company, Philadelphia, Pennsylvania.

Nanda, N., and Gramiak, R., 1978. Clinical Echocardiography. The C.V. Mosby Co. St. Louis, Missouri.

Nelson, R., and Couto, G., 1986. Essentials of Small Animal Internal Medicine. Mosby Year Book. Boston, Massachusetts.

Nickel R., Schummer, A., and Seiferle, E. 1981. The Anatomy of the Domestic Animals: The Circulatory System, the Skin and The Cutaneous Organs of the Domestic Mammals. Verlag Paul Parey. Berlin, Hamburg.

Norton. H., 1982. Biomedical Sensors: Fundamentals and Applications. Noyes Publications. New Jersey.

Pagani, M., Israel, M., Baig, H., Manders, T., Kerkhof,, P., and Vatner, S., 1979. Effect of Age on Aortic Pressure-Diameter and Elastic Stiffness-Stress Relationships in Unanesthetized Sheep. *Circulation Research.*; 44: 420 -429.

Pipers,F., Bonagura, J., Hamlin, R., and Kittleson, M., 1979. Echocardiographic Abnormalities of the Mitral Valve Associated with Left-Side Heart Diseases in the Dog. *JAVMA.*; 6: 580-586.

Redo, S., and Ecker, R., 1966. The Use of an Adhesive in Cardiovascular Surgery. *Archives Surgery.*; 319-322.

Sahn, D., DeMaria, A., Kisslo, J., and Weyman, A., 1978. Recommendations Regarding Quantitation in M-mode Echocardiography: Results of a survey of Echocardiographic Measurement. *Circulation.*; 58: 1072 -1083.

Teodori, M. F., Rodgers, V.G.J., Brant, A.M., Borovetz, H.S., Webster, M.W., Steed, D.L. and Peitzman, A.B. 1986. Effect of Compliance and Diameter on Stress at Arterial Anastomoses. *Current Surgery.*; 1968; 54:505-508.

Termini, B. and Lee, Y., 1976. Essentials of Echocardiography. Medical Economics Books Division. New Jersey.

Vatner, S., Pasipoularides, A., and Mirsky, I., 1984. Measurement of Arterial Pressure-Dimension Relationships in Conscious Animals. *Annals of Biomedical Engineering.*; 12: 521-534.

Voros, K., Holmes, J., and Gibbs, C., 1991. Measurement of Cardiac Dimensions with Two-dimensional Echocardiography in the Living Horse. *Equine Veterinary Journal.*; 26: 461-465.

Webster, J., 1978. Medical Instrumentation: Application and Design. Houghton Mifflin and Co. Boston, Massachusetts.

Wells, P., 1972. Ultrasound in Clinical Diagnosis. Churchill Livingstone. London, England.

Woodcock, J., 1976. Clinical Blood Flow Measurement. Sector Publishing Limited. London, England.

Yamakoshi, K., Rolfe, P. and Murphy, C. 1988. Current Development in Non-invasive Measurement of Arterial Blood Pressure. *Journal of Biomedical Engineering.*; 1 10:130-137.

ACKNOWLEDGMENTS

This research project would not have been possible without the guidance and support of Dr. Richard L. Engen. I would like to express my sincere gratitude and appreciation to Dr. Engen in taking time from his responsibilities and always being there for consultation throughout the whole experiment.

In addition, I would like to thank my program of study committee. Thanks to Dr. Mary Helen Greer for always having a helping hand and a smile while I was trying to write this thesis, and for her enormous contribution in advising me during the research process. Thanks to Dr. Frederick Hembrough for his numerous advice regarding the experimental protocol and design, and for his ability to challenge me to understand the physiological concepts underlying this research.

I would also like to thank Dr. Kristina Miles for her willingness to help me during the experimental part of this thesis and for being available for consultation afterwards.

Finally, I will like to thank God, for always being there in moments of uncertainty, and for always guiding me through even the toughest days. Last but not least, I would like to thank all those people that in one way or another helped me go through this unforgettable journey. This research project is yours too!

APPENDIX A: SPECIFICATIONS

Apogee

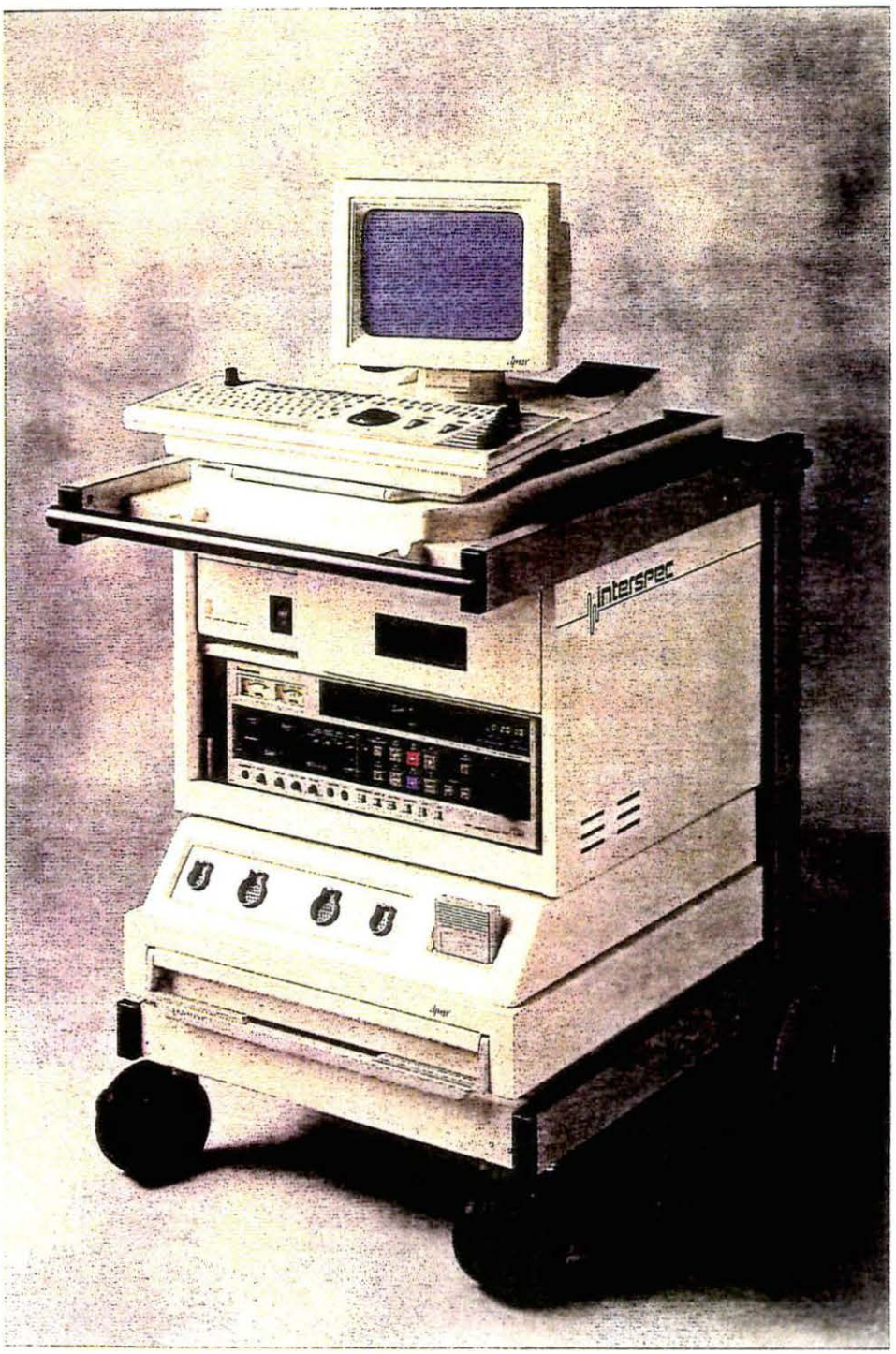

Apogee Specifications

Integrated Patient Reports

Cardiac 2-D Sector and M-Mode Reports include: volumes, ejection fraction, cardiac output, body surface area, stroke volume, cardiac index, percent area change, mean VCF, fractional shortening, leaflet excursion, ejection periods, ratios

Cardiac Doppler Report: includes mean and maximum velocity and pressure, acceleration, time, pressure half-time, valve area, flow velocity integral, acceleration time, cardiac output, stroke volume, cardiac index, continuity equation, ratios.

Vascular Report: includes percent narrowing by distance and area, volume flow, ICA/CCA ratios in diastole and systole, pulsatility index, damping factor

Options

Videocassette recorders
High-resolution video printers
Apogee cart with isolation transformer
Footswitch
Duplex and Doppler-only probes 2 to 10 MHz

Physical Data

Main Unit

width - 21 in / 53.5 cm
height- 9.5in / 24 cm
depth - 23 in / 58.5
weight- 42 pounds / 19 Kg
User Interface (keyboard-monitor module)
width - 20 in / 51 cm
height- 12 in /30.5
depth - 19 in/ 48cm
weight- 24 pounds / 11 Kg

Apogee Cart

without User Interface module
width - 25.5 in / 65 cm
height- 32.5in / 82.5 cm
depth - 19.5 / 75 cm

with User Interface module
width - 25.5 / 65 cm
height- 44.5 / 113 cm
depth - 29.5 / 75 cm

Electrical Service

Requirements: 50/60 Hz, 110/120 VAC, 220/240 VAC
Power Consumption 800 watts

Environmental Requirements

Operating temperature: 0 to 40 C
Storage temperature: -30 to + 55 C
Relative humidity (non-condensing): 5 to 95 %
Operating altitude: 12,000 feet maximum
Non-operating altitude: 12,000 feet maximum or pressurized shipping container

Standards Compliance

Designed to meet or exceed performance and safety requirements of UL 544 and IEC 601

Specifications are subject to change without notice.

APPENDIX B: DOG #1

Dog #1 **Date:** **Oct. 19, 1994**

I.D. #:	163
Sex:	Female
Weight:	49
Length:	41
Breed	Chow X
Strain	Red

A. Non-Invasive

M-Mode

Trial #	Systole	Diastole	Heart Rate	Notes:
1	2.2	2.2	126	Freq: 7.5 MHz
2	2.1	2.2	126	IPWR 50 %
3	2.1	2.1	126	Depth 8.0 cm
4	1.8	2.2	119	
5	1.8	2.2	119	Zoom Function
6	2	2.2	119	D=2.5 - 6.5 cm
7	1.9	2.2	119	
8	2	2.2	94	From left side
9	1.9	2	79	

2-D View

Trial #	Systole	Diastole	Heart Rate	Notes:
1	1.9	2.1	98	
2	1.8	2.1	91	
3	1.8	2	69	
4	1.8	2	69	
5	2	2.1	69	From left side

B. Invasive

M-Mode

Trial #	Systole	Diastole	Heart Rate	Notes:
1	1.6	1.7	128	Zoom Function
2	1.9	1.8	124	D=0.0 - 3.0 cm
3	1.9	1.9	124	Freq: 9 MHz
4	1.8	1.8	125	D= 4 cm

2-D View

Trial #	Systole	Diastole	Heart Rate	Notes:
1	1.7	1.7	121	Freq: 9MHz
2	1.7	1.7	121	IPWR 100 %
3	1.8	1.7	126	D= 4 cm

APPENDIX C: DOG #2

Dog # 2 **Date:** **Oct. 26, 1994**

I.D. #	96
Sex	Male
Weight (Lb)	41
Length (in)	36
Breed/Strain	Brittany X

A. Non-Invasive

M-Mode

Trial #	Systole	Heart Rate
1	1.9	65
2	1.9	65
3	2.1	134
4	2.1	134

Mech. Diam: 1.74 cm

Trial #	Diastole	Heart Rate
1	2.1	65
2	2.1	65
3	2	134
4	2.1	134
5	1.6	134

2-D View

Trial#	Systole	Heart Rate
1	1.6	138
2	1.6	138
3	1.8	134
4	1.8	57
5	1.8	126

Trial#	Diastole	Heart Rate
1	2	134
2	1.8	57
3	1.9	57
4	1.5	57

B. Invasive

M-Mode View

Trial #	Systole (cm)	Heart Rate
1	1.9	153
2	2.3	150
3	2.2	150
4	1.8	152

Trial #	Diastole (cm)	Heart Rate
1	2	153
2	2.2	150
3	2.2	150
4	2	152

2-D View

Trial #	Systole (cm)	Heart Rate
1	1.6	172
2	1.6	172
3	1.7	144
4	1.7	144
5	1.7	144
6	1.7	144

Trial #	Diastole (cm)	Heart Rate
1	1.5	172
2	1.6	172
3	1.9	144
4	1.9	144
5	1.6	144
6	1.6	144

APPENDIX D: DOG #3

Dog #3

Date: Nov. 2, 1994

I.D. #	196
Sex	Female
Weight (lb)	25
Length (in)	34
Breed/Strain	Lab X

A. Non-Invasive

M-mode

Trial #	Systole	Heart Rate
1	1.7	106
2	1.7	106
3	1.7	106
4	1.7	87
5	1.7	87
6	1.7	87
7	1.8	87
8	1.9	87

Trial #	Diastole	Heart Rate
1	1.7	106
2	1.9	106
3	1.8	106
4	1.8	87
5	1.7	87
6	1.8	87
7	1.8	87
8	1.9	87

2-D View

Trial #	Systole	Heart Rate
1	1.7	117
2	1.8	117
3	1.7	117
4	1.7	139

Trial#	Diastole	Heart Rate
1	1.8	117
2	1.8	117
3	1.8	117
4	2	139

B. Invasive

M-mode

Trial #	Systole	Heart rate
1	1.7	211
2	1.9	211
3	1.8	211
4	1.7	211
5	1.9	211
6	1.8	211
7	1.5	183
8	1.5	183

Trial #	Diastole	Heart Rate
1	2	211
2	2	211
3	2	211
4	1.9	211
5	1.9	211
6	1.5	183
7	1.6	183
8	1.6	183

2-D View

Trial #	Systole	Heart Rate
1	1.5	197
2	1.5	197
3	1.6	208
4	1.6	208
5	1.7	208
6	1.5	197
7	1.5	197

Trial #	Diastole	Heart Rate
1	1.3	197
2	1.3	197
3	1.6	208
4	1.5	208
5	1.4	208
6	1.5	197
7	1.4	197

APPENDIX E: DOG #4

Dog # 4 Date: Nov. 17, 1994

I.D. #	70
Sex	Male
Weight (Kg)	12.25 Kg
Length (in)	
Breed/Strain	

A. Non-Invasive

M-Mode

# Meas.	Systole	Heart Rate
1	1.7	165
2	1.6	160

# Meas.	Diastole	Heart Rate
1	1.8	165
2	1.8	165

2-D View

# Meas.	Systole	Heart Rate
1	1.4	149
2	1.4	149
3	1.4	149
4	1.4	149
5	1.3	142
6	1.3	142

#Meas.	Diastole	Heart Rate
1	1.5	149
2	1.5	149
3	1.5	149
4	1.5	149
5	1.5	149
6	1.4	149
7	1.3	142
8	1.4	142
9	1.4	142
10	1.4	142

B. Non-Invasive **15% TBV**

M-Mode

#Meas.	Systole	Heart Rate
1	1.5	147
2	1.5	147

#Meas.	Diastole	Heart Rate
1	1.5	147
2	1.4	147

2-DView

#Meas.	Systole	Heart Rate
1	1.4	146
2	1.3	146
3	1.3	153
4	1.3	153
5	1.2	155
6	1.2	155

#Meas.	Diastole	Heart Rate
1	1.3	146
2	1.3	146
3	1.2	146
4	1.3	153
5	1.3	153
6	1.3	153
7	1.3	153
8	1.3	153
9	1.2	155
10	1.1	155

C. Non-Invasive **30% TBV**

M-Mode

#Meas.	Systole	Heart Rate
1	1.4	138
2	1.3	138

#Meas.	Diastole	Heart Rate
1	1.3	138
2	1.2	138

2-D View

#Meas.	Systole	Heart Rate
1	1	134
2	1	134

#Meas.	Diastole	Heart Rate
1	1.1	134
2	1.1	134
3	1.1	135
4	1.1	135

D. Invasive **30% TBV**

M-Mode

#Meas.	Systole	Heart Rate
1	1	155
2	1.1	155
3	1.1	155
4	1.1	155

#Meas.	Diastole	Heart Rate
1	1.1	155
2	1.1	155
3	1.1	155
4	1.1	155

2-D View

#Meas.	Systole	Heart Rate
1	1.2	160
2	1.2	160
3	1.2	153
4	1	153
5	1	134

#Meas.	Diastole	Heart Rate
1	1.1	160
2	1.2	160
3	1.1	153
4	1.2	153
5	1.1	134

E. Mechanical measurement **1.1 cm**

APPENDIX F: DOG #5

Dog # 5 Date: Nov. 29, 1994

I.D. #	63
Sex	Male
Weight (Kg)	12.25 Kg
Length (in)	
Breed/Strain	

A. Non-Invasive

M-Mode

# Meas.	Systole	Heart Rate
1	1.4	103
2	1.4	103
3	1.5	88

# Meas.	Diastole	Heart Rate
1	1.7	103
2	1.4	103
3	1.8	88
4	1.6	88

2-D View

# Meas.	Systole	Heart Rate
1	1.6	79
2	1.6	79
3	1.5	79
4	1.6	75
5	1.6	75

#Meas.	Diastole	Heart Rate
1	1.5	79
2	1.7	79
3	1.7	75
4	1.4	75
5	1.5	75

B. Non-Invasive **15% TBV**

M-Mode

#Meas.	Systole	Heart Rate
1	1.4	129
2	1.4	149
3	1.4	139

#Meas.	Diastole	Heart Rate
1	1.5	129
2	1.6	149
3	1.7	139

2-DView

#Meas.	Systole	Heart Rate
1	1.4	111
2	1.5	111
3	1.4	111
4	1.5	122
5	1.4	122

#Meas.	Diastole	Heart Rate
1	1.5	111
2	1.5	111
3	1.4	111
4	1.5	122
5	1.3	122

C. Non-Invasive **30% TBV**

M-Mode

#Meas.	Systole	Heart Rate
1	1	150
2	1.4	150
3	1.5	135
4	1.4	105

#Meas.	Diastole	Heart Rate
1	1.2	150
2	1.2	150
3	1.1	150
4	1.2	150
5	1.1	150
6	1.2	150
7	1.2	135
8	1.2	135
9	1.2	135
10	1.5	135
11	1.4	105
12	1.4	105

2-D View

#Meas.	Systole	Heart Rate
1	1.2	142
2	1.2	142
3	1.3	128
4	1.2	128

#Meas.	Diastole	Heart Rate
1	1.1	142
2	1.2	142
3	1.2	142
4	1.2	142
5	1.2	128
6	1.4	128
7	1.3	128

D. Invasive **30% TBV**

M-Mode

#Meas.	Systole	Heart Rate
1	1	135
2	1.1	132
3	1.1	132
4	1.2	132

#Meas.	Diastole	Heart Rate
1	1.2	135
2	1.3	132
3	1.2	132
4	1.2	132

2-D View

#Meas.	Systole	Heart Rate
1	1.2	152
2	1.2	152
3	1.3	135
4	1.3	111
5	1.4	111

#Meas.	Diastole	Heart Rate
1	1.1	153
2	1.2	135
3	1.2	135
4	1.3	111
5	1.2	111

E. Mechanical measurement **1.22**

APPENDIX G: DOG #6

Dog #6 Date: Dec. 7, 1994

I.D. #	257
Sex	Male
Weight (Lb)	41
Length (in)	38
Breed	Shep XX

A. Non-Invasive

M-Mode

#Meas.	Systole	Heart Rate
1	1.8	114
2	1.5	115
3	1.2	115
4	1.3	97
5	1.2	97
6	1.3	97

#Meas.	Diastole	Heart Rate
1	1.9	114
2	1.8	114
3	1.7	114
4	1.7	115
5	1.8	97
6	1.8	97

2-D View

#Meas.	Systole	Heart Rate
1	1.6	125
2	1.6	125
3	1.7	125
4	1.6	105
5	1.4	97

#Meas.	Diastole	Heart Rate
1	1.9	125
2	1.9	125
3	1.8	105
4	1.6	97
5	1.6	97

B. Invasive **Baseline**

M-Mode

#Meas.	Systole	Heart Rate
1		183
2		183
3		158
4		158
5		149

#Meas.	Diastole	Heart Rate
1	1.8	153
2	1.8	153
3	1.8	153
4	1.9	153
5	1.8	153

2-D View

#Meas.	Systole	Heart Rate
1	1.6	183
2	1.9	183
3	1.7	158
4	1.7	158
5	1.8	149

#Meas.	Diastole	Heart Rate
1	1.5	183
2	1.6	183
3	1.6	158
4	1.5	158
5	1.4	149

C. Invasive

15% TBV

M-Mode

#Meas.	Systole	Heart Rate
1		
2		
3		
4		
5		
6		

#Meas.	Diastole	Heart Rate
1	1.5	138
2	1.4	138
3	1.5	138
4	1.5	138
5	1.6	136
6	1.6	136
7	1.5	136
8	1.6	136

2-D View

#Meas.	Systole	Heart Rate
1	1.1	155
2	1.3	155
3	1.1	155

#Meas.	Diastole	Heart Rate
1	1.1	155
2	1.2	155
3	1.1	155

D. Invasive **30% TBV**

M-Mode

#Meas.	Systole	Heart Rate
1	1.1	124
2	1.1	124

#Meas.	Diastole	Heart Rate
1	1.1	124
2	1.1	124
3	1.1	124
4	1	124

2-D View

#Meas.	Systole	Heart Rate
1	1.2	156
2	1	156
3	1.2	122
4	1.1	122

#Meas.	Diastole	Heart Rate
1	1.1	156
2	1.1	156
3	1.1	156
4	1.1	122

Mechanical **Measuremen** 1.43 cm

APPENDIX H: DOG #7

Dog #7 Date: Dec. 14, 1994

I.D. #	245
Sex	Male
Weight (Lb)	31
Length (in)	38
Breed	Beagle-X

A. Non-Invasive

M-Mode

#Meas.	Systole	Heart Rate
1	1.8	115
2	1.8	115
3	1.8	115
4	1.7	115
5	1.6	130

#Meas.	Diastole	Heart Rate
1	1.9	115
2	2	115
3	1.9	115
4	1.9	115
5	1.9	130
6	1.9	130

2-D View

#Meas.	Systole	Heart Rate
1	2.2	110
2	2.1	110
3	1.9	101
4	1.9	101

#Meas.	Diastole	Heart Rate
1	2.2	110
2	2	110
3	2	110
4	1.9	101
5	1.8	101

B. Invasive **Baseline**

M-Mode

#Meas.	Systole	Heart Rate
1	1.8	110
2	1.8	110

#Meas.	Diastole	Heart Rate
1	2.1	110
2	2	110
3	2	110
4	2.1	110
5	2.1	110
6	2.1	110

2-D View

#Meas.	Systole	Heart Rate
1	1.6	113
2	1.6	113

#Meas.	Diastole	Heart Rate
1	1.8	113
2	1.8	113

C. Invasive **15% TBV**

M-Mode

#Meas.	Systole	Heart Rate
1	1.3	132
2	1.3	132

#Meas.	Diastole	Heart Rate
1	1.5	132
2	1.5	132
3	1.5	132
4	1.4	132

2-D View

#Meas.	Systole	Heart Rate
1	1	144
2	1	144
3	1.1	144

#Meas.	Diastole	Heart Rate
1	1.1	144
2	1.1	144
3	1	144

D. Invasive **30% TBV**

M-Mode

#Meas.	Systole	Heart Rate
1	1.1	135
2	1.1	135

#Meas.	Diastole	Heart Rate
1	1.3	135
2	1.2	135
3	1.3	135

2-D View

#Meas.	Systole	Heart Rate
1	1.2	127
2	1.2	127

#Meas.	Diastole	Heart Rate
1	1.3	127
2	1.3	127
3	1.3	127
4	1.3	127

Mechanical **Measurement** 1.2